Structure and Dynamics of a Synthetic O-Glycosylated Cyclopeptide in Solution Determined by NMR Spectroscopy and MD Calculations

H. Kessler,*,† H. Matter,† G. Gemmecker,† M. Kottenhahn,† and J. W. Bats‡

Contribution from the Organisch-Chemisches Institut, Technische Universität München, Lichtenbergstrasse 4, D-8046 Garching, Germany, and Institut für Organische Chemie der Johann Wolfgang Goethe-Universität, Niederurseler Hang, D-6000 Frankfurt/Main, Germany.
Received May 17, 1991

Abstract: Conformational analysis by NMR spectroscopy and restrained molecular dynamics (MD) of the O-glycosylated cyclic hexapeptide cyclo(D-Pro[1]-Phe[2]-Ala[3]-Ser[4][*O*-2-deoxy-D-lactopyranosyl-α-(1–3)]-Phe[5]-Phe[6]) (**I**) and the cyclic hexapeptide precursor cyclo(D-Pro[1]-Phe[2]-Ala[3]-Ser[4]-Phe[5]-Phe[6]) (**II**) is described. For **II**, an X-ray structure was obtained and compared with the structure in solution. For both compounds, the distance constraints derived from 2D NMR measurements could not be completely satisfied by a single conformation, but distance violations occurred only in the Phe[5] region of the peptide. The specific pattern of NOE-derived distances in this part of the molecule suggested an equilibrium between two conformers containing βI- and βII-type turns, respectively, with Phe[5] at $i + 2$. MD simulations with time-dependent distance constraints support the assumption of a βI/βII flip in **I** and **II**. The conformations were refined using restrained MD simulations in vacuo, in water, and in DMSO. To study the exoanomeric effect of β(1–4)- and α-glycosidic linkages on conformation, new force field parameters derived from literature data were incorporated, leading to greater flexibility and significantly populated alternate conformers around the β(1–4)-glycosidic bond, in agreement with literature data. The α-glycosidic linkage connecting the disaccharide moiety to the peptide prefers only one conformation. Both **I** and **II** have similar backbone conformations and hydrogen-bonding patterns. Therefore, the O-glycosylation does not affect the conformation or the overall shape of the peptide backbone or side chains.

1. Introduction

Glycoproteins are involved in important biological processes such as cell recognition,[1] differentiation, growth, control, and export processes; they are also responsible for the specification of blood groups.[2] Furthermore, they play a critical role in cell–cell interactions and the response of cells to the external environment (in which biologically active substances such as hormones, antigens, and toxins[3] are contained). Despite their biological importance, very little is known about the influence of the carbohydrate on protein conformation.[4] For a rational design of glycopeptide pharmaceuticals, a knowledge of the spatial structures is essential.[5] Toward this goal, we have initiated a synthetic and structural investigation of glycopeptides.[6]

Several experimental techniques indicate a stiffening of the peptide chain containing a carbohydrate-linked amino acid.[7] In *O*-glycopeptides the first sugar is linked to a serine, threonine, hydroxylysine, or hydroxyproline.[8] These amino acids are often involved in reverse-turn structures in peptides and proteins.[9] Most of the glycosylated amino acid residues are located in the $i + 1$ or $i + 2$ position of β-turn structures of glycoproteins.[10]

Here we report the results from a study of a cyclic hexapeptide with and without O-glycosylation: cyclo(D-Pro[1]-Phe[2]-Ala[3]-Ser[4][*O*-2-deoxy-D-lactopyranosyl-α-(1–3)]-Phe[5]-Phe[6]) (**I**) and cyclo(D-Pro[1]-Phe[2]-Ala[3]-Ser[4]-Phe[5]-Phe[6]) (**II**) (Figure 1). Crystals of **II** suitable for X-ray diffraction methods were obtained, and the solid-state structure was compared with the conformation observed in solution. We have chosen the model compound cyclo(D-Pro[1]-Phe[2]-Ala[3]-Ser[4]-Phe[5]-Phe[6]) (**II**) for our study for several reasons. The serine hydroxyl group is located in the $i + 1$ position of a reverse β-turn,[11] and therefore this side chain functionality is exposed to the solvent and provides an ideal target for direct glycosylation. The cyclic peptide has reduced conformational flexibility, and reliable conformational analysis is possible. The structure of **I** is similar to the cyclic *N*-glycopeptide recently studied.[6d] In addition, the peptide is a cyclic retro analogue of the peptide hormone somatostatin. Several cyclopeptides similar in structure have been examined (ref 12 and references cited therein).

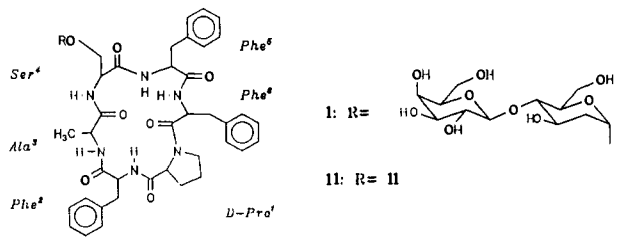

Figure 1. Constitution of glycopeptide **I** and cyclic hexapeptide **II**.

† Technische Universität München.
‡ Johann Wolfgang Goethe-Universität.

(1) (a) Feizi, T. *Nature* **1985**, *314*, 53–57. (b) Feizi, T.; Childs, R. A. *Biochem. J.* **1987**, *245*, 1–11. (c) Goldstein, E. J. *ACS Symp. Ser.* **1979**, *88*. (d) Olden, K.; Bernard, B. A.; White, S. L.; Parent, J. B. *J. Cell Biochem.* **1982**, *18*, 313–335.
(2) Sharon, N.; Lis, H. *Chem. Eng. News* **1981**, March 30, 21–44.
(3) Hughes, R. C. *Essays Biochem.* **1975**, *11*, 1–36.
(4) (a) Ishii, H.; Inoue, Y.; Chujo, R. *Int. J. Pept. Protein Res.* **1984**, *24*, 421–429. (b) Narasinga Rao, B. N.; Bush, C. A. *Biopolymers* **1987**, *26*, 1227–1244. (c) Bush, C. A.; Feeney, R. E. *Int. J. Pept. Protein Res.* **1986**, *28*, 386–397. (d) Gerken, T. A.; Butenhof, K. J.; Shogren, R. *Biochemistry 1989*, *28*, 5536–5543. (e) Shogren, R.; Gerken, T. A.; Jentoft, N. *Biochemistry* **1989**, *28*, 5525–5536. (f) Taupipat, N.; Mattice, W. L. *Biopolymers* **1990**, *29*, 377–383. (g) Gerken, T. A.; Dearborn, D. G. *Biochemistry* **1984**, *23*, 1485–1497. (h) Gerken, T. A.; Jentoft, N. *Biochemistry* **1987**, *26*, 4689–4699. (i) Gerken, T. A. *Arch. Biochem. Biophys.* **1986**, *247*, 239–253. (j) Mimura, Y.; Inoue, Y.; Joe Maeji, N.; Chujo, R. *Int. J. Pept. Protein Res.* **1989**, *34*, 363–368. (k) Hollosi, M.; Perczel, A.; Fasman, G. D. *Biopolymers* **1990**, *29*, 1549–1564.
(5) Perun, T. J.; Propst, C. L., Eds.; *Computer-Aided Drug Design*; Marcel Dekker: New York, 1989.
(6) (a) Kessler, H.; Kling, A.; Kottenhahn, M. *Angew. Chem., Int. Ed. Engl.* **1990**, *29*, 425–427. (b) Kottenhahn, M.; Kessler, H. *Liebigs Ann. Chem.* **1991**, 727–744. (c) Kessler, H.; Kottenhahn, M.; Kling, A.; Kolar, C. *Angew. Chem., Int. Ed. Engl.* **1987**, *26*, 888–890. (d) Kessler, H.; Matter, H.; Gemmecker, G.; Kling, A.; Kottenhahn, M. *J. Am. Chem. Soc.* **1991**, *113*, 7550–7563. (e) Kessler, H.; Kottenhahn, M.; Kling, A.; Matter, H. *Proceedings of the 3rd Akabori Conference*, German–Japanese Symposium on Peptide Chemistry, July 2–5, 1989, Prien/Chiemsee FRG; Wünsch, E., Ed.; Martinsried FRG 1989, pp 45–49.
(7) Bush, C. A.; Ralapati, S.; Matson, G. M.; Yamasaki, R. D.; Osuga, D. T.; Yeh, Y.; Feeney, R. E. *Arch. Biochem. Biophys.* **1984**, *232*, 624–631.

0002-7863/92/1514-4805$03.00/0

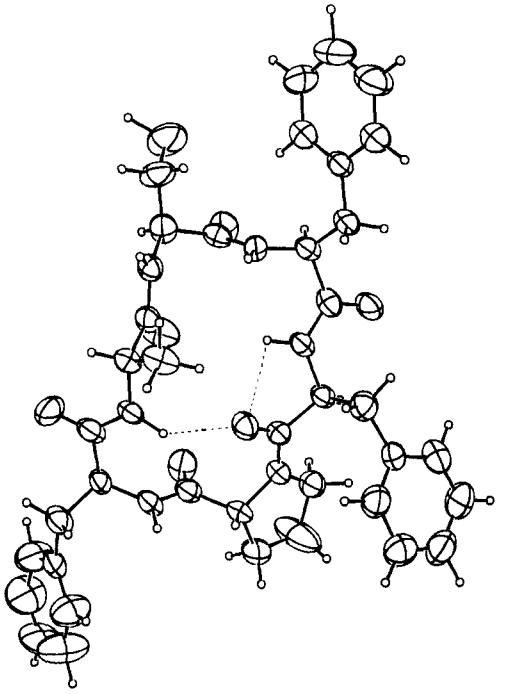

Figure 2. Perspective view of peptide **II** observed in the crystal structure with 50% probability ellipsoids.

2. Results

A. X-ray Structure Determination of II. Crystals of **II** suitable for X-ray diffraction were obtained from a saturated solution in DMSO. The resulting crystal structure is shown in Figure 2. All peptide bonds are trans. The molecule is approximately rectangular in shape with D-Pro[1], Phe[2], Ser[4], and Phe[5] at the four corners. Similar conformations were observed in the crystal structures of cyclo(D-Pro-Phe-Phe-Pro-Phe-Phe)[13] and cyclo(D-Pro-Phe-Thr-Phe-Trp-Phe).[14] The residues D-Pro[1] and Phe[2] are part of a βII′-turn which accommodates a hydrogen bond between Ala[3]NH and Phe[6]C=O. The residues Ser[4] and Phe[5] are part of a βI-turn, although there is no hydrogen bond between Phe[6]NH and Ala[3]C=O [a distance of 294 pm for H···O]. The Phe[2]NH is involved in intermolecular hydrogen bonding to a neighboring molecule, whereas Ser[4]NH, Ser[4]OH, and Phe[5]NH are each hydrogen-bound to a DMSO molecule. The five-membered D-Pro ring is planar, which is physically unrealistic. However, the large displacement parameters of D-Pro[1]C_γ in a direction perpendicular to the ring show the proline ring to be disordered between the exo and endo C_γ-envelope conformations.

B. NMR Measurements. For the glycopeptide **I**, the NMR measurements were carried out at a proton frequency of 600 MHz to resolve the resonances of the disaccharide unit. The measurements for **II** were carried out at 250 MHz. The ^{1}H resonances for both **I** and **II** were assigned using a combination of TOCSY with different mixing times[15] and DQF-COSY.[16] From an inverse

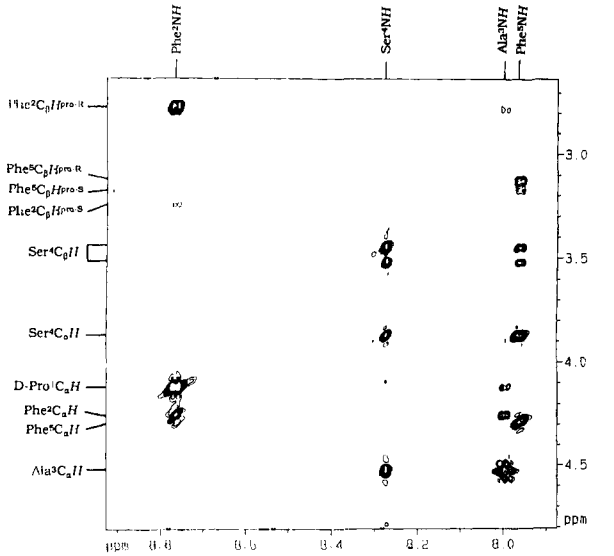

Figure 3. NH/$C_\alpha H$ region of the 600-MHz NOESY spectrum (120 ms mixing time, no zero-quantum suppression) of the glycopeptide **I** in DMSO-d_6. Only positive contours are shown.

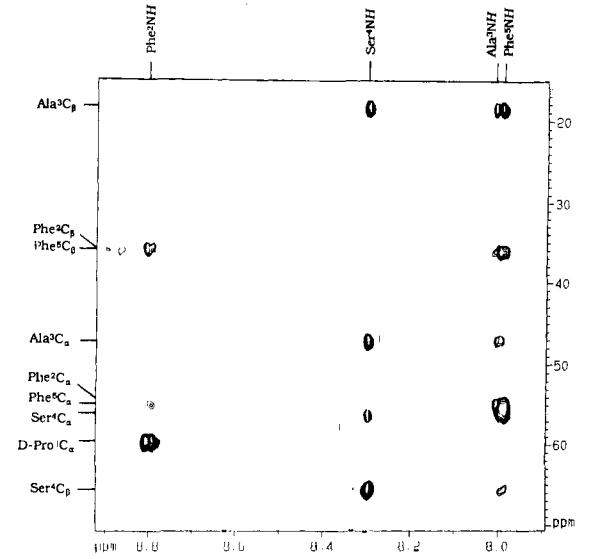

Figure 4. NH/C_α region of the natural abundance 600-MHz ^{13}C-HMQC-NOESY spectrum (200 ms mixing time) of the glycopeptide **I** in DMSO-d_6.

^{13}C–^{1}H shift correlation (HMQC[17]) and an HMQC-TOCSY[18] the complete assignment of all ^{13}C resonances was carried out. The chemical shifts of the ^{1}H and ^{13}C resonances of **I** and **II** are summarized in Table I. The sequential assignment was achieved from the analysis of NOESY[19] and ROESY[20] spectra. An ad-

(8) Neuberger, A.; Gottschalk, A.; Marshall, R. D.; Spiro, R. A. *Glycoproteins: Their Composition, Structure and Function*; Gottschalk, A., Ed.; Elsevier: New York, 1972; Vol. 5A, pp 450–490.
(9) Chou, P.; Fasman, R. D. *J. Mol. Biol.* **1977**, *115*, 135–175.
(10) (a) Aubert, J.-P.; Biserte, A.; Loucheux-Lefebvre, M. H. *Arch. Biochem. Biophys.* **1976**, *175*, 410–418. (b) Beeley, J. G. *Biochem. Biophys. Res. Commun.* **1977**, *76*, 1051–1056. (c) Mononen, I.; Karjalainen, E. *Biochim. Biophys. Acta* **1984**, *788*, 364–367.
(11) (a) Rose, G. D.; Gierasch, L. M.; Smith, J. A. *Adv. Protein Chem.* **1985**, *37*, 1–109. (b) Smith, J. A.; Pease, L. G. *CRC Crit. Rev. Biochem.* **1980**, *8*, 315–399.
(12) Kessler, H.; Anders, U.; Schudok, M. *J. Am. Chem. Soc.* **1990**, *112*, 5908–5916.
(13) Kessler, H.; Klein, M.; Müller, A.; Wagner, K.; Bats, J. W.; Ziegler, K.; Frimmer, M. *Angew. Chem., Int. Ed. Engl.* **1986**, *25*, 997–999.
(14) Kessler, H.; Bats, J. W.; Griesinger, C.; Koll, S.; Will, M.; Wagner, K. *J. Am. Chem. Soc.* **1988**, *110*, 1033–1049.
(15) (a) Braunschweiler, L.; Ernst, R. R. *J. Magn. Reson.* **1983**, *53*, 521–528. (b) Bax, A.; Byrd, R. A.; Aszalos, A. *J. Am. Chem. Soc.* **1984**, *106*, 7632–7633. (c) Bax, A.; Davis, D. G. *J. Magn. Reson.* **1985**, *65*, 355–360.
(16) (a) Piantini, U.; Sørensen, O. W.; Ernst, R. R. *J. Am. Chem. Soc.* **1982**, *104*, 6800–6801. (b) Rance, M.; Sørensen, O. W.; Bodenhausen, G.; Wagner, G.; Ernst, R. R.; Wüthrich, K. *Biochem. Biophys. Res. Commun.* **1983**, *117*, 458–479.
(17) (a) Müller, L. *J. Am. Chem. Soc.* **1979**, *101*, 4481–4484. (b) Bax, A.; Griffey, R. H.; Hawkins, L. B. *J. Magn. Reson.* **1983**, *55*, 301–315.
(18) (a) Lerner, A.; Bax, A. *J. Magn. Reson.* **1986**, *69*, 375–380. (b) Kessler, H.; Bermel, W.; Griesinger, C. Presented at the Sixth Meeting of the Fachgruppe Magnetic Resonance Spectroscopy, Berlin, September 25–28, 1985.
(19) Jeener, J.; Meier, B. H.; Bachmann, P.; Ernst, R. R. *J. Chem. Phys.* **1979**, *71*, 4546–4553.
(20) (a) Bothner-By, A. A.; Stephens, R. L.; Lee, J.; Warren, C. D.; Jeanloz, R. W. *J. Am. Chem. Soc.* **1984**, *106*, 811–813. (b) Bax, A.; Davis, D. G. *J. Magn. Reson.* **1985**, *63*, 207–213. (c) Kessler, H.; Griesinger, C.; Kerssebaum, R.; Wagner, K.; Ernst, R. R. *J. Am. Chem. Soc.* **1987**, *109*, 607–609.

Table I. NMR Chemical Shifts of I and II in DMSO-d_6 at 300 K[a]

	I(^{1}H)	II(^{1}H)	I(^{13}C)	II(^{13}C)
D-Pro^1-C=O			171.5	171.5
D-Pro^1-C$_\alpha$H	4.10	4.08	59.7	59.6
D-Pro^1-C$_\beta$H$^{pro\text{-}R}$	1.44	1.40	28.1	28.1
D-Pro^1-C$_\beta$H$^{pro\text{-}S}$	1.63	1.60		
D-Pro^1-C$_\gamma$H$^{pro\text{-}R}$	1.38	1.30	24.5	24.4
D-Pro^1-C$_\gamma$H$^{pro\text{-}S}$	1.83	1.78		
D-Pro^1-C$_\delta$H$^{pro\text{-}R}$	2.76	2.65	46.7	46.6
D-Pro^1-C$_\delta$H$^{pro\text{-}S}$	3.33	3.28		
Phe^2-C=O			170.8	170.8
Phe^2-NH	8.75 (−5.8)	8.73 (−6.9)		
Phe^2-C$_\alpha$H	4.23	4.20	54.5	54.5
Phe^2-C$_\beta$H$^{pro\text{-}R}$	2.75	2.72	35.9	35.9
Phe^2-C$_\beta$H$^{pro\text{-}S}$	3.23	3.20		
Ala^3-C=O			172.8	172.8
Ala^3-NH	7.98 (−1.8)	7.95 (−2.1)		
Ala^3-C$_\alpha$H	4.51	4.48	47.2	54.4
Ala^3-C$_\beta$H	1.47	1.41	18.3	18.2
Ser^4-C=O			170.2	169.7
Ser^4-NH	8.28 (−4.4)	8.15 (−6.4)		
Ser^4-C$_\alpha$H	3.85	3.70	56.1	58.9
Ser^4-C$_\beta$H^b	3.50	3.50	65.5	60.2
	3.42	3.31		
Ser^4-OH		4.96		
Phe^5-C=O			170.6	170.6
Phe^5-NH	7.97 (−4.8)	7.68 (−3.9)		
Phe^5-C$_\alpha$H	4.27	4.30	54.8	54.4
Phe^5-C$_\beta$H$^{pro\text{-}R}$	3.11	3.05	36.0	36.3
Phe^5-C$_\beta$H$^{pro\text{-}S}$	3.18	3.14		
Phe^6-C=O			168.4	168.4
Phe^6-NH	7.42 (−0.9)	7.22 (0.0)		
Phe^6-C$_\alpha$H	4.65	4.60	53.2	53.2
Phe^6-C$_\beta$H$^{pro\text{-}S}$	2.78	2.68	38.1	38.2
Phe^6-C$_\beta$H$^{pro\text{-}R}$	3.07	3.10		
2-deoxyGlc-C$_{(1)}$H	4.77		97.0	
2-deoxyGlc-C$_{(2)}$H^{eq}	1.99		36.4	
2-deoxyGlc-C$_{(2)}$H^{ax}	1.41			
2-deoxyGlc-C$_{(3)}$H	3.75		66.3	
2-deoxyGlc-C$_{(4)}$H	3.28		81.9	
2-deoxyGlc-C$_{(5)}$H	3.44		71.1	
2-deoxyGlc-C$_{(6)}$H^{eq}	3.72		60.2	
	3.65			
2-deoxyGlc-O$_{(3)}$H	4.52			
2-deoxyGlc-O$_{(6)}$H	4.54			
Gal-C$_{(1)}$H	4.22		103.8	
Gal-C$_{(2)}$H	3.36		70.7	
Gal-C$_{(3)}$H	3.34		73.3	
Gal-C$_{(4)}$H	3.63		68.2	
Gal-C$_{(5)}$H	3.46		75.5	
Gal-C$_{(6)}$H^b	3.49		60.4	
	3.54			
Gal-O$_{(2)}$H	5.05			
Gal-O$_{(3)}$H	4.73			
Gal-O$_{(4)}$H	4.48			
Gal-O$_{(6)}$H	4.63			

[a] All data are given in ppm. Temperature gradients of N*H* protons [ppb/K] are given in parentheses. [b] No diastereotopic assignment.

ditional verification was obtained from a selective inverse ^{13}C–^{1}H long-range correlation (HMBC[21]) with a 270° Gaussian pulse for semisoft excitation (HMBCS[22]). This technique was also applied for the diastereotopic assignment of the C$_\beta$ protons. With known C$_\alpha$H–C$_\beta$H coupling constants, a calculation of peak intensities yields a reliable discrimination between heteronuclear antiperiplanar and synclinal coupling from the HMBCS.[23]

Only one distinct set of signals was found in the ^{1}H and ^{13}C NMR spectra of I and II. No conformational change slow on the NMR time scale could be detected by line-broadening effects.

Table II. ^3J(N*H*,C$_\alpha$*H*) Coupling Constants (Hz) for I and II and Calculated Dihedral Angles

	Phe^2	Ala^3	Ser^4	Phe^5	Phe^5
			Peptide I		
$^3J_{NH,\alpha}$[a]	9.0	9.4	3.9	8.2	7.0
φ_{exp}[b]	−139.3	−134.5	−174.0	−146.7	−154.7
	−100.7	−105.5	−66.0	−93.3	−85.3
			105.2		80.0
			14.8		40.0
			Peptide II		
$^3J_{NH,\alpha}$[a]	8.9	10.2	3.8	7.7	6.4
φ_{exp}[b]	−139.8	−129.9	−174.7	−150.3	−158.8
	−100.2	−118.1	−65.3	−89.7	−81.2
			106.0	71.3	86.3
			14.0	48.7	33.7

[a] Experimental values determined from the 1D spectrum after resolution enhancement. [b] Possible values for the peptide backbone angles φ (deg) from Bystrov's Karplus equation (the following parameters were used: $A = 9.4$, $B = -1.1$, $C = 0.4$).

Table III. ^3J(C$_\alpha$*H*,C$_\beta$*H*) Coupling Constants (Hz) and Calculated Populations (%) for the Side Chain Conformers of I and II

residue	Phe^2	Phe^5	Phe^6
	Peptide I		
^3J(C$_\alpha$*H*,C$_\beta$*H*$^{pro\text{-}R}$)	11.8	9.3[a]	4.5
^3J(C$_\alpha$*H*,C$_\beta$*H*$^{pro\text{-}S}$)	3.2	5.1[a]	9.3
$\chi_1 = -60°$	84	61	17
$\chi_1 = 180°$	5	23	60
$\chi_1 = 60°$	11	16	23
	Peptide II		
^3J(C$_\alpha$*H*,C$_\beta$*H*$^{pro\text{-}R}$)	11.7	9.2[a]	4.4
^3J(C$_\alpha$*H*,C$_\beta$*H*$^{pro\text{-}S}$)	3.2	4.8[a]	9.0
$\chi_1 = -60°$	82	60	17
$\chi_1 = 180°$	5	20	58
$\chi_1 = 60°$	13	20	25

[a] Coupling constants checked and verified by simulation using the SMART program because of strongly coupled spin systems.

All other conventional criteria for conformational homogeneity were also fulfilled.[24] However, as was reported recently, these observations cannot exclude the occurrence of rapidly interconverting conformers.[6d,25]

Interproton distances were obtained from a NOESY experiment with a mixing time of 100 ms and a ROESY spectrum with a mixing time of 150 ms. The peak volumes were integrated on both sides of the diagonal. The distance restraints were derived from the integrals using the assumption of isotropic tumbling and the isolated two-spin approximation (ISPA).[26] The ROESY-derived distances were corrected to account for offset effects.[27] The integrals between geminal protons served as a reference for calibration. For II the Phe^{2}N*H*–D-Pro^{1}C$_\alpha$*H* crosspeak was used for calibration with a distance of 207 pm (derived from X-ray crystallography), an approach that has been successfully applied to other cyclic peptides.[28]

(21) Bax, A.; Summers, M. F. *J. Am. Chem. Soc.* **1986**, *108*, 2093–2094.
(22) (a) Bermel, W.; Wagner, K.; Griesinger, C. *J. Magn. Reson.* **1989**, *83*, 223–232. (b) Emsley, L.; Bodenhausen, G. *J. Magn. Reson.* **1989**, *82*, 211–221. (c) Kessler, H.; Schmieder, P.; Köck, M.; Kurz, M. *J. Magn. Reson.* **1990**, *88*, 615–618.
(23) Hofmann, M.; Gehrke, M.; Bermel, W.; Kessler, H. *Magn. Reson. Chem.* **1989**, *27*, 877–886.
(24) (a) Kessler, H.; Bermel, W.; Müller, A.; Pook, K. H. In *The Peptides, Analysis, Synthesis, Biology*; Udenfriend, S., Meienhofer, J., Hruby, V. R., Eds.; Verlag Chemie: Weinheim, 1986; Vol. 7, pp 437–472. (b) Kessler, H.; Bermel, W. *Methods in Stereochemical Analysis*; Croasmun, W. R., Marchand, P., Eds.; VCH: Deerfield Beach, FL, 1987; Vol. 9, pp 259–299. (c) Kessler, H. *Angew. Chem., Int. Ed. Engl.* **1982**, *21*, 512–523.
(25) (a) Kessler, H.; Bats, J. W.; Lautz, J.; Müller, A. *Liebigs Ann. Chem.* **1989**, 913–928. (b) Kessler, H.; Griesinger, C.; Lautz, J.; Müller, A.; van Gunsteren, W. F.; Berendsen, H. J. C. *J. Am. Chem. Soc.* **1988**, *110*, 3393–3396. (c) Kopple, K. D.; Bhandary, K. K.; Kartha, G.; Wang, Y. S.; Parameswaran, K. N. *J. Chem. Soc.* **1986**, *108*, 4637–4642. (d) Kopple, K. D.; Wang, Y. S.; Cheng, A. G.; Bhandary, K. K. *J. Am. Chem. Soc.* **1988**, *110*, 4168–4176. (e) Stradley, S. J.; Rizo, J.; Bruch, M. D.; Stroup, A. N.; Gierasch, L. M. *Biopolymers* **1990**, *29*, 263–287. (f) Rowan, R.; Warshel, A.; Sykes, B. D.; Karplus, M. J. *Biochemistry* **1974**, *13*, 970–981.
(26) Neuhaus, D.; Williamson, M. *The Nuclear Overhauser Effect in Structural and Conformational Analysis*; VCH: Weinheim, 1989.
(27) Griesinger, C.; Ernst, R. R. *J. Magn. Reson.* **1987**, *75*, 261–271.
(28) Kessler, H.; Kerssebaum, R., Klein, A. G.; Obermeier, R.; Will, M. *Liebigs Ann. Chem.* **1989**, 269–294.

Table IV. Selected Experimental Proton–Proton Distances (pm) for Glycopeptide I and Cyclic Peptide II in Comparison with Distances for Ideal Type βI- and βII-Turns

protons		I	II	βI	βII
Phe^5NH	$Phe^5C_\alpha H$	241	218	280–300	200–220
Phe^5NH	$Phe^5C_\beta H^{pro\text{-}R}$	285	299	240–260[a]	340–360[a]
Phe^5NH	$Phe^5C_\beta H^{pro\text{-}S}$	341	347	340–360[a]	380–410[a]
Phe^5NH	Phe^6NH	231	239	290–320	260–290
Phe^5NH	$Ser^4C_\alpha H$	242	230	340–360	200–220

[a] Given for $\chi_1 = -60°$ for amino acid in position $i + 2$ of a turn.

To obtain NOEs of the overlapping proton resonances of the O-glycosylated hexapeptide, the recently described HMQC-NOESY was carried out.[29] The NOEs are separated by the large chemical shift dispersion of the ^{13}C resonances and can easily be recognized. The $NH/C_\alpha H$ region of an HMQC-NOESY spectrum in natural ^{13}C abundance for the glycopeptide I is shown in Figure 4, in comparison to the NOESY spectrum in Figure 3.

The temperature coefficients of amide proton chemical shifts indicate *intra*molecular hydrogen bonds for Phe^6NH and Ala^3NH and an external orientation for Phe^2NH, Ser^4NH, and Phe^5NH for I and II (Table I).[24c] The $^3J(NH,C_\alpha H)$ coupling constants were extracted from 1D spectra after resolution enhancement; they provide information about dihedral angles via the Karplus equation (Table II).[24c,30]

The populations of side chain χ_1 rotamers were determined via $^3J(C_\alpha H,C_\beta H)$ coupling constants (Table III).[31,32] These coupling constants were extracted from ECOSY spectra[33] for Phe^2, Phe^5, and Phe^6. For I and II, the $Phe^5C_\beta H$ protons formed a strongly coupled spin system; therefore, simulations using the program SMART[34] were carried out to evaluate the coupling constants. The diastereotopic assignment was carried out by interpretation of NOE effects[35] and homonuclear $^3J(NH,C_\beta H)$ and heteronuclear $^3J(C{=}O,C_\beta H)$ coupling constants.[31]

C. Conformational Analysis. With these NOEs and temperature coefficients a crude model can be built. The intramolecular hydrogen bonds involving Phe^6NH and Ala^3NH suggest a hexapeptide structure consisting of two β-turns for both compounds. Between D-Pro^1 ($i + 1$) and Phe^2 ($i + 2$) a βII′-turn structure is supported by the characteristic NOEs for this secondary structure element. However, in the other half of the molecule at Ser^4-Phe^5 it is not possible to find a *single* turn structure which fits all of the experimental data.

A close look at the distance constraints reveals several inconsistencies, all involving Phe^5NH (cf. Table IV). For the glycopeptide I, for example, the distance between Phe^5NH and $Ser^4C_\alpha H$ is only compatible with a βII-turn between Ala^3 and Phe^6 (allowing for a 10% error). On the other hand, the experimental value for the distance Phe^5NH–$Phe^5C_\beta H^{pro\text{-}S}$ corresponds clearly to a βI-turn. Furthermore, several other NOE effects result in distances that lie in between the values for ideal βI- and βII-turns (e.g., Phe^5NH–$Phe^5C_\beta H^{pro\text{-}R}$ and Phe^5NH–$Phe^5C_\alpha H$).

A similar situation is observed in the case of II: the distance Phe^5NH–$Phe^5C_\beta H^{pro\text{-}S}$ fits into a βI-turn as observed in the crystal structure; however, the Phe^5NH–$Phe^5C_\alpha H$ and Phe^5NH–$Ser^4C_\alpha H$ distances are only compatible with a βII-turn. Again, other NOEs yield distances between the ideal values for βI- and βII-turns (e.g., Phe^5NH–$Phe^5C_\beta H^{pro\text{-}R}$).

These inconsistencies cannot be fully explained by experimental errors, since conformational studies of a large number of similar systems yield interproton distances deviating less than 10% from the NOE-derived distances.[6d,12,14,26] In addition, a closer look at the NOE distance deviations for I and II reveals the existence of a well-defined part of the structure consisting of the βII′-turn region (rms deviations of 20–30 pm, i.e., <10%) and much higher deviations in the Phe^5-Ser^4 region (rms values >50 pm) (cf. Table VI).

We therefore conclude that the NOE data for both I and II cannot be fulfilled by a single conformation, but only by an averaging between two (or more) conformations[6d,25] with differences in the Phe^5-Ser^4 region. In the following molecular dynamics studies, it will be shown that the assumption of a fast exchange between a βI- and βII-turn between Ser^4 and Phe^5 is already sufficient to explain all experimental data.

It should be mentioned here that homonuclear $^3J(NH,C_\alpha H)$ coupling constants are not very helpful in this case, since they are compatible with both β-turn structures (cf. Table II). This experimental parameter, frequently overemphasized, is ambiguous because small fluctuations in the torsion angle φ often occuring in cyclic peptides can greatly change the coupling constant,[6d] rendering it rather useless for an exact conformational analysis. However, the existence of an HMBC crosspeak between $Ser^4C{=}O$ and $Phe^5C_\alpha H$ indicates a significant population of the βII-turn, where the involved nuclei are *antiperiplanar* to each other.

D. Molecular Dynamics Simulations. All molecular dynamics (MD) simulations were carried out with the GROMOS program[36] on Silicon Graphics 4D/240SX and 4D/70GTB computers. Starting structures were generated using INSIGHT (BIOSYM). The solid-state structure of II with βII′/βI-turns served as the starting structure for I and II. The amide bonds were assumed to be in the trans configuration, since there is no experimental indication of a cis configuration; the differences in the ^{13}C chemical shift of D-$ProC_\beta$ and D-$ProC_\gamma$ resonances and the NOEs are consistent with trans peptide bonds.[12,24c,37] The side chains of the Phe residues were fixed in the dominating population (Table III).[14] To account for solvation during the in vacuo simulations, the charges of the solvent-exposed amide protons and nitrogens were reduced using the temperature gradients of the NH resonances (Table I).[14]

A harmonic potential was employed for upper and lower distance restraints. The function switches from harmonic to linear when the deviation is greater than 10% from the target distance. The lower bound distances are given in Tables VI and VII; for the upper bounds, 100 and 90 pm were added for each methyl group and nonstereospecifically assigned CH_2 group, respectively.[36d] For all other NOEs, the lower and upper bounds were set to the same value.[14] The choice of moderate force constants for the subsequent refinement procedure allows for certain deviations of the actual from the experimental distances (e.g., 2000 kJ mol^{-1} nm^{-2} corresponds to an energy of $kT/2$ for a 35-pm deviation from the target value). The kinetic energy was included by coupling the whole system to a thermal bath.[38] All MD simulations were

(29) (a) Shon, K.; Opella, S. J. *J. Magn. Reson.* **1989**, *82*, 193–197. (b) Crouch, R. C.; Andrews, C. W.; Martin, G. E.; Luo, J. K.; Castle, R. N. *Magn. Reson. Chem.* **1990**, *28*, 774–778. (c) Crouch, R. C.; McFadyen, R. B.; Daluge, S. M.; Martin, G. E. *Magn. Reson. Chem.* **1990**, *28*, 792–796.

(30) (a) Karplus, M. J. *J. Chem. Phys.* **1959**, *30*, 11–15. (b) Bystrov, V. F. *Prog. Nucl. Magn. Reson. Spectrosc.* **1976**, *10*, 41–81.

(31) (a) Kessler, H.; Griesinger, C.; Wagner, K. *J. Am. Chem. Soc.* **1987**, *109*, 6927–6933. (b) Anders, U.; Gemmecker, G.; Kessler, H.; Griesinger, C. *Fresenius Z. Anal. Chem.* **1987**, *327*, 72–73.

(32) (a) Pachler, K. G. R. *Spectrochim. Acta* **1963**, *19*, 2085–2092. (b) Pachler, K. G. R. *Spectrochim. Acta* **1964**, *20*, 581–587.

(33) (a) Griesinger, C.; Sørensen, O. W.; Ernst, R. R. *J. Am. Chem. Soc.* **1985**, *107*, 6394–6396. (b) Griesinger, C.; Sørensen, O. W.; Ernst, R. R. *J. Chem. Phys.* **1986**, *85*, 6837–6852.

(34) Studer, W. J. *J. Magn. Reson.* **1988**, *77*, 424–438.

(35) Wagner, G.; Braun, W.; Havel, T. F.; Schaumann, T.; Go, N.; Wüthrich, K. *J. Mol. Biol.* **1987**, *196*, 611–639.

(36) (a) Åqvist, J.; van Gunsteren, W. F.; Leijonmark, M.; Tapia, O. J. *J. Mol. Biol.* **1985**, *183*, 461–477. (b) van Gunsteren, W. F.; Kaptein, R.; Zuiderweg, E. R. P. *Proceedings of the NATO/CECAM Workshop on Nucleic Acid Conformation and Dynamics*; Olsen, W. K., Ed.; Orsay, 1983, pp 79–92. (c) van Gunsteren, W. F.; Boelens, R.; Kaptein, R.; Scheek, R. M.; Zuiderweg, E. R. P. *Molecular Dynamics and Protein Structure*; Hermans, J., Ed.; Polycrystal Book Service: Western Springs, IL, 1985; pp 92–99. (d) B. V. Biomos, Nijenborgh 16 NL 9747 AG Groningen, Groningen Molecular Simulation (GROMOS) Library Manual, van Gunsteren, W. F., Berendsen, H. J. C. GROMOS User's Manual, pp 1–229.

(37) (a) Mierke, D. F.; Yamazaki, T.; Said-Nejad, O. E.; Felder, E. R.; Goodman, M. *J. Am. Chem. Soc.* **1989**, *111*, 6847–6849. (b) Bairaktari, E.; Mierke, D. F.; Mammi, S.; Peggion, E. *J. Am. Chem. Soc.* **1990**, *112*, 5383. (c) Deber, C. M.; Madison, V.; Blout, E. R. *Acc. Chem. Res.* **1976**, *9*, 106–113. (d) Siemion, I. Z.; Wieland, T.; Pook, K. H. *Angew. Chem., Int. Ed. Engl.* **1975**, *14*, 702–703.

(38) Berendsen, H. J. C.; Postma, J. P. M.; van Gunsteren, W. F.; Di Nola, A.; Haak, J. R. *J. Chem. Phys.* **1984**, *81*, 3684–3690.

Table V. New Additional GROMOS Force Field Parameters for α- and β-Glycosidic Linkages in Oligosaccharides and Glycopeptides[a]

bond types		K_r	r_e
α-glycoside	$C^1{}_\alpha$–$O^1{}_\alpha$	600	141.1
	$O^1{}_\alpha$–$C^X{}_\alpha$	600	144.0
β-glycoside	$C^1{}_\beta$–$O^1{}_\beta$	600	139.0
	$O^1{}_\beta$–$C^X{}_\beta$	600	144.0
angle types		K_θ	θ_e
α-glycoside	$C^1{}_\alpha$–$O^1{}_\alpha$–C^X	65	115.00
	O^5–$C^1{}_\alpha$–$O^1{}_\alpha$	80	111.55
β-glycoside	$C^1{}_\beta$–$O^1{}_\beta$–C^X	65	116.40
	C^5–$C^1{}_\beta$–$O^1{}_\beta$	80	107.40
dihedral angle types		K_n	n	δ
α-glycoside	O^5–$C^1{}_\alpha$–$O^1{}_\alpha$–C^X	2.15	1	300
	C^2–$C^1{}_\alpha$–$O^1{}_\alpha$–C^X	0.85	3	0
	C^2–$C^1{}_\alpha$–$O^1{}_\alpha$–C^X	1.75	2	300
β-glycoside	O^5–$C^1{}_\beta$–$O^1{}_\beta$–C^X	−1.05	1	0
	C^2–$C^1{}_\beta$–$O^1{}_\beta$–C^X	1.40	3	0
	C^2–$C^1{}_\beta$–$O^1{}_\beta$–C^X	1.25	2	120

[a] The following symbols were used: K_r, force constant for bonds (kcal mol^{-1} Å^{-2}); r_e, bond length (Å); K_θ, force constant for angles (kcal mol^{-1} rad^{-2}]; θ_e, bond angle (deg); K_n, force constant for dihedral angles (kcal mol^{-1}); n, multiplicity; δ, phase shift (deg).

carried out with the application of SHAKE;[39] the step size for the integration of Newton's equation (leap-frog algorithm[39]) was 2 fs (for the in vacuo calculations) or 1 fs (for the calculations in water and in DMSO).

The GROMOS force field can be used for studies of oligosaccharides or glycopeptides.[40] Although previous investigations on oligosaccharides without implementation of the exoanomeric effect have reproduced experimental results, this stereoelectronical effect was added as a dihedral torsion potential in the potential energy function. The origin of this effect is the bonding interaction of the lone pair orbital into the σ^* orbital of the antiperiplanar C–X bond,[41] which influences oligosaccharide conformations.[42,43] The minimum energy value for the glycosidic angle H^1–C^1–O^1–C^X is close to +60° for α-D-glycosides and close to −60° for β-D-glycosides.[44] The glycosidic dihedral angles are defined as follows: φ, O^5–C^1–O^1–$C^{4'}$ and ψ, C^1–O^1–$C^{4'}$–$C^{3'}$ according to Sundaralingam[45] and Bush et al.[46] (following IUPAC convention in which right-handed rotation corresponds to positive dihedral angles[47]). There is some discrepancy in the rotational barriers: ab initio studies on dimethoxymethane as a model system by Wiberg and Murcko[48] suggest that the rotational barriers of the glycosidic dihedral angles are significantly lower than those calculated earlier by Jeffrey et al.[44] To account for this effect, some new parameters were included in the GROMOS force field. The bond length C^1–$O^{4'}$ ($O^{4'}$ = O^1) and the valence angles O^5–C^1–$O^{4'}$ and C^5–O^5–C^1 depend on the anomeric configuration.[44,49] Hence, these values were adjusted to the mean crystallographic values for α- and β-glycosidic linkages.[44] According to Homans' parametrization of the AMBER force field[50] for φ, an additional torsional potential was applied. The corresponding ψ angle is only dominated by nonbonded interactions.[42c] Furthermore, Homans' study has shown reasonable agreemnt between simulated and experimental conformational properties without inclusion of explicit torsional terms for ψ.[50] The differences between torsion energies for dimethoxymethane from the quantum mechanics and molecular mechanics calculations were fit to relatively simple functions in order to reproduce the minimum energies correctly.[48,50] The new parameters are given in Table V.

i. MD Simulations of I in Vacuo, in Water, and in DMSO. The initial velocities for the atoms were taken from a Maxwell distribution at the corresponding temperature. During the first picosecond, the system was strongly coupled to a 1000 K temperature bath[38] with a temperature relaxation time of 0.01 ps and a force constant for the distance restraints of 4000 kJ mol^{-1} nm^{-2} (K_{dc}). In the next 4 ps, the temperature was scaled down to 300 K and the temperature relaxation time was increased to 0.1 ps. The values for K_{dc} were decreased to 2000 kJ mol^{-1} nm^{-2}. After 10 ps of equilibration, structures were saved for analysis over 40 and 80 ps time spans with K_{dc} = 2000 kJ mol^{-1} nm^{-2}.

Preliminary MD simulations for testing the carbohydrate force field in vacuo indicated that the Coulombic interactions were overemphasized when the full charges of the carbohydrate residues were used, as given in refs 36d and 40a. This leads to very strained global structures with many hydrogen bonds between the peptide and disaccharide units. All experimental data are very poorly fulfilled. A reduction of these charges by 75% results in reasonable structures in the in vacuo simulations which, in addition, show great correspondence to structures obtained by MD simulations in aqueous surroundings and in DMSO (see below). All in vacuo simulations were carried out with reduced charges, whereas simulations in water and in DMSO used the full saccharide charges. A critical overview of the importance and the difficulties for the derivation of charges for such systems has been given elsewhere.[42b]

Two different simulations for each conformer (with a βII- and a βI-turn between Ser^4-Phe^5) were performed, one with the new parametrization of the force field and one without accounting for the exoanomeric effect, each starting from the same minimized structure. After 10 ps of equilibration, 80-ps trajectories were calculated for each conformer with and without implementation of the exoanomeric effect in the potential energy function (K_{dc} = 2000 kJ mol^{-1} nm^{-2}). For distinguishing the different simulations, the following abbreviations will be used: **MDI^{v1}** = without exoanomeric effect, starting from βI-turn; **MDI^{v1e}** = with exoanomeric effect, starting from βI-turn; **MDI^{v2}** = without exoanomeric effect, starting from βII-turn; **MDI^{v2e}** = with exoanomeric effect, starting from βII-turn (v vs s = in vacuo or in water; 1 vs 2 = type of β-turn; e = with exoanomeric effect). Two NOEs in contradiction to a βI-turn structure were omitted from the distance constraint list (indicated in Table VI) for the refinement of this βI-turn structure. The resulting conformations were further refined by MD simulations in H_2O and in DMSO. The development of potential energy parameters for DMSO[51] within the GROMOS force field was reported recently.[52] In addition, these simulations enables us to check the effect of the reduced carbohydrate charges in the in vacuo calculations.

The averaged and minimized structures from the in vacuo simulations were used as starting structures for the water and

(39) (a) Ryckaert, J. P.; Cicotti, C.; Berendsen, H. J. C. *J. Comput. Phys.* **1977**, *23*, 327–343. (b) van Gunsteren, W. F.; Berendsen, H. J. C. *Mol. Phys.* **1977**, *34*, 1311–1327.

(40) (a) Köhler, J. E. H.; Saenger, W.; van Gunsteren, W. F. *Eur. Biophys. J.* **1987**, *15*, 197–210. (b) Köhler, J. E. H.; Saenger, W.; van Gunsteren, W. F. *Eur. Biophys. J.* **1987**, *15*, 211–224. (c) Köhler, J. E. H.; Saenger, W.; van Gunsteren, W. F. *Eur. Biophys. J.* **1988**, *16*, 153–168. (d) Köhler, J. E. H.; Saenger, W.; van Gunsteren, W. F. *J. Mol. Biol.* **1988**, *203*, 241–250. (e) Köhler, J. E. H.; Saenger, W.; van Gunsteren, W. F. *J. Biomol. Struct. Dyn.* **1988**, *6*, 181–198.

(41) (a) Kirby, A. J. *The Anomeric Effect and Related Stereoelectronic Effects at Oxygen*; Springer: Berlin, 1983. (b) Lemieux, R. U.; Koto, S. *Tetrahedron* **1974**, *30*, 1933–1944. (c) Lemieux, R. U. *Pure Appl. Chem.* **1971**, *25*, 527–548. (d) Tvaroska, I.; Bleha, T. *Adv. Carbohydr. Chem. Biochem.* **1989**, *47*, 45.

(42) (a) Meyer, B. *Top. Curr. Chem.* **1990**, *154*, 141–208. (b) Homans, S. W. *Prog. NMR Spectrosc.* **1990**, *22*, 55–81. (c) Bock, H. *Pure Appl. Chem.* **1983**, *55*, 605–622. (d) Paulsen, H. *Angew. Chem., Int. Ed. Engl.* **1990**, *29*, 823–839.

(43) (a) Thøgersen, H.; Lemieux, R. U.; Bock, K.; Meyer, B. *Can. J. Chem.* **1982**, *60*, 44–57. (b) Lemieux, R. U.; Bock, K.; Delbaere, L. T. J.; Koto, S.; Rao, V. S. *Can. J. Chem.* **1980**, *58*, 631–653.

(44) Jeffrey, G. A.; Pople, J. A.; Binkley, J. S.; Vishveshwara, S. *J. Am. Chem. Soc.* **1978**, *100*, 373–379.

(45) Sundaralingam, M. *Biopolymers* **1968**, *6*, 189–213.

(46) Bush, C. A.; Yan, Z.-Y.; Rao, B. N. *J. Am. Chem. Soc.* **1986**, *108*, 6168–6173.

(47) IUPAC-IUB Commision on Biochemical Nomenclature. *Eur. J. Biochem.* **1983**, *131*, 5–7.

(48) Wiberg, K. B.; Murcko, M. A. *J. Am. Chem. Soc.* **1989**, *111*, 4821–4828.

(49) Berman, H.; Chu, S.; Jeffrey, G. A. *Science* **1967**, *157*, 1576.

(50) Homans, S. W. *Biochemistry* **1990**, *29*, 9110–9118.

(51) Rao, B. G.; Singh, U. C. *J. Am. Chem. Soc.* **1990**, *112*, 3802–3811.

(52) Mierke, D. F.; Kessler, H. *J. Am. Chem. Soc.* **1991**, *113*, 9466–9470.

Table VI. Comparison of Experimental and Calculated Proton–Proton Distances for Glycopeptide I[a]

protons		NOESY	MDI^{s2e}	MDI^{sle}	MDI$_{av}$[e]	MDI^{tNOE}
Phe^{5}N*H*	Phe^{5}C$_\alpha$*H*	241[d]	204	268	232	252
Phe^{5}N*H*	Phe^{5}C$_\beta$*H*$^{pro\text{-}R}$	285	355	239	291	287
Phe^{5}N*H*	Phe^{5}C$_\beta$*H*$^{pro\text{-}S}$	341	403	345	373	369
Phe^{5}N*H*	Phe^{6}N*H*	231	320	286	297	284
Phe^{5}N*H*	Ser^{4}N*H*	393	443	368	403	390
Phe^{5}N*H*	Ser^{4}C$_\alpha$*H*	242[d]	201	363	280	313
Phe^{5}N*H*	Ser^{4}C$_\beta$*H*	312[b]	347	314	328	336
Phe^{5}C$_\alpha$*H*	Phe^{5}C$_\beta$*H*$^{pro\text{-}S}$	262	249	255	250	243
Phe^{6}N*H*	Phe^{6}C$_\alpha$*H*	281	281	281	275	277
Phe^{6}N*H*	Phe^{6}C$_\beta$*H*$^{pro\text{-}R}$	307	296	305	292	323
Phe^{6}N*H*	Phe^{6}C$_\beta$*H*$^{pro\text{-}S}$	298	316	288	298	283
Phe^{6}N*H*	Ala^{3}C$_\beta$*H*	350[c]	437	407	416	425
Phe^{6}N*H*	Phe^{5}C$_\alpha$*H*	319	337	335	333	328
Phe^{6}C$_\alpha$*H*	Phe^{6}C$_\beta$*H*$^{pro\text{-}R}$	262	259	247	252	235
Phe^{6}C$_\alpha$*H*	D-Pro^{1}C$_\delta$*H*	222[b]	222	222	206	224
D-Pro^{1}C$_\alpha$*H*	D-Pro^{1}C$_\beta$*H*	238[b]	242	244	239	243
Phe^{2}N*H*	Ala^{3}N*H*	255	245	256	246	246
Phe^{2}N*H*	D-Pro^{1}C$_\beta$*H*	381[b]	389	390	381	393
Phe^{2}N*H*	Phe^{2}C$_\beta$*H*$^{pro\text{-}R}$	245	232	234	226	246
Phe^{2}N*H*	Phe^{2}C$_\beta$*H*$^{pro\text{-}S}$	346	346	347	342	353
Phe^{2}N*H*	Phe^{2}C$_\alpha$*H*	306	276	274	272	278
Phe^{2}N*H*	D-Pro^{1}C$_\alpha$*H*	208	208	208	202	210
Ala^{3}N*H*	Ala^{3}C$_\alpha$*H*	336	283	286	282	285
Ala^{3}N*H*	D-Pro^{1}C$_\alpha$*H*	348	372	369	365	366
Ala^{3}N*H*	Ala^{3}C$_\beta$*H*	252	274	282	274	288
Ala^{3}N*H*	Phe^{2}C$_\alpha$*H*	307	342	336	335	324
Ala^{3}N*H*	Phe^{2}C$_\beta$*H*$^{pro\text{-}R}$	315	288	304	289	326
Ser^{4}N*H*	D-Pro*H*^{2eq}	445	471	469	457	454
Ser^{4}N*H*	Ala^{3}C$_\alpha$*H*	244	236	240	235	246
Ser^{4}N*H*	Ser^{4}C$_\alpha$*H*	269	270	257	262	255
Ser^{4}N*H*	Ala^{3}C$_\beta$*H*	255[c]	350	343	343	355
Ser^{4}N*H*	Ser^{4}C$_\beta$*H*	246[b]	291	293	287	300
Ser^{4}N*H*	D-Glc*H*^{1}	384	455	451	445	430
Ser^{4}C$_\alpha$*H*	Ser^{4}C$_\beta$*H*	297[b]	253	258	252	254
D-Glc*H*^{1}	Ser^{4}C$_\alpha$*H*	335	382	396	381	392
D-Glc*H*^{1}	Ser^{4}C$_\beta$*H*	311[b]	376	363	363	369
Gal*H*^{1}	D-Glc*H*^{4}	212	220	260	228	248
			rms Deviations (pm)			
NOEs involving Phe^{5}N*H* (1–7)			56	55	30	34
all other NOEs (8–37)			24	25	23	23
complete set of NOEs (1–37)			33	33	25	26

[a] All values are given in pm. For the notation of the different MD trajectories, please see text. [b] Increased by 90 pm for MD run (CH_2 without diastereotopic assignment[36b]). [c] Increased by 100 pm for MD run (CH_3 group[36b]). [d] NOEs omitted in the MD run MDI^{sle} (see text). [e] MDI$_{av}$ indicates averaging over both trajectories, MDI^{sle} and MDI^{s2e}.

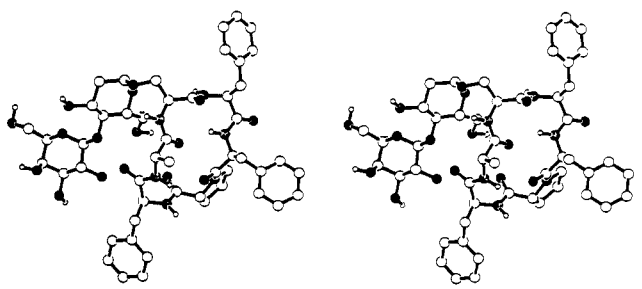

Figure 5. Stereoview of the mean structure of peptide I with a βII-turn in the Ala^3 to Phe^6 region, obtained from averaging the 60-ps trajectory from MDI^{s2e} (in water) and five steps of restrained energy minimization with the same force constant as applied in the MD simulation. The protons bound to carbon are not shown.

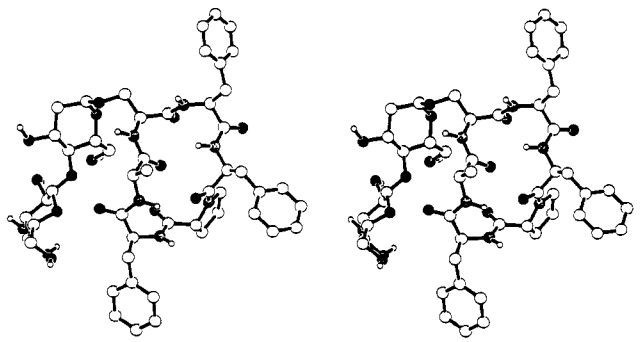

Figure 6. Stereview of the mean structure of peptide I with a βI-turn in the Ala^3 to Phe^6 region, obtained from averaging the 60-ps trajectory from MDI^{s1e} (in water) and five steps of restrained energy minimization with the same force constant as applied in the MD simulation. The protons bound to carbon are not shown.

DMSO simulations. The structures were placed in the middle of truncated octahedrons[53] with the following numbers of solvent molecules: MDI^{v2e}, 464 in 15.08 nm^3 = MDI^{s2e} in water, and 164 in 21.04 nm^3 = MDI^{d2e} in DMSO; MDI^{v1e}, 470 in 15.13 nm^3 = MDI^{sle} in water, and 151 in 19.57 nm^3 = MDI^{dle} in DMSO; MDI^{v2}, 566 in 18.17 nm^3 = MDI^{s2} in water; MDI^{v1}, 583 in 18.73 nm^3 = MDI^{s1} in water. The water molecules are modeled by the simple rigid three point charge model.[54] The simulations in water were performed without SHAKE, while the calculations in DMSO were performed with SHAKE. A cut-off radius of 1 nm was used for the nonbonded interactions. All simulations were performed at 300 K with K_{dc} = 1000 kJ mol^{-1} nm^{-2}. The solvent was allowed to relax by 500 steps of EM while the position of the solute atoms

(53) Adams, D. J. *J. Chem. Phys. Lett.* **1979**, *62*, 329–332.

(54) Berendsen, H. J. C.; Postma, J. P. M.; van Gunsteren, W. F.; Hermans, J. *Intermolecular Forces*; Pullman, B., Ed.; Reidel: Dordrecht, 1981; pp 331–342.

was fixed, followed by 500 steps EM without restraint of the solute. The simulations in water were performed with 5 ps for equilibration and then 60 ps for analysis; the simulations in DMSO were run with 80 ps for analysis. The side chain dihedrals were not fixed due to damped mobility in the solvent surroundings.[55] During the time scale of all simulations, no conformational change of the peptide backbone occurred.

The two different structures **MDI**^{s1e} and **MDI**^{s2e}, each obtained by averaging over the 60-ps MD trajectory in water followed by energy minimization, are shown in Figures 5 and 6. The average distances and dihedral angles for both structures are given in Tables VI and VIII (all distances were calculated for each time step of the trajectory and subsequently averaged[56] because of the nonlinear dependence between spectroscopic data and geometric parameters[57,58]); the hydrogen bonds are summarized in the supplementary material. Table X gives a comparison of glycosidic bond dihedral angles obtained from different simulations.

ii. Results. The simulations for **I** in vacuo, in water, and in DMSO lead to very similar structures of the glycopeptide. In the following discussion, we will focus on the calculations in water; however, the NOE violations are the same for the simulations in DMSO and in vacuo.

The averaged structure **MDI**^{s2e} satisfies 33 of the 37 distance constraints: those in violation all involve Phe^{5}N*H* as described above (cf. Table VI). These NOEs deviate significantly from the observed distances in this model. In contrast to this part of the molecule, all distances in the stable βII′-turn are fulfilled. The rms deviation for the NOEs involving Phe^{5}N*H* is 56 pm, while for the rest of the molecule a value of 24 pm is found (Table VI), demonstrating that the distance violations in the Phe^5 region cannot be explained by experimental errors.

The distance constraints in violation in **MDI**^{s2e} are satisfied in the time-averaged structure **MDI**^{s1e}, but now two other constraints also involving Phe^{5}N*H* are violated. The proposed conformations **MDI**^{s2e} and **MDI**^{s1e} differ in the φ and ψ dihedral angles around the central amide bond in the β-turn between Ser^4 and Phe^5. This leads to different β-turn structures in this half of the molecule, as expected from an analysis of the distances, which are not in agreement with a single ideal β-turn structure.

However, *all* NOEs can be explained with the assumption of two different conformations in equilibrium with a βI- and a βII-turn. This corresponds to an average **MDI**$_{av}$ over the two corresponding simulations **MDI**^{s2e} and **MDI**^{s1e}. As shown in Table VI, the rms deviations for **MDI**$_{av}$ are reduced dramatically for the NOEs involving Phe^{5}N*H* (from 55 and 56 pm down to 30 pm in **MDI**$_{av}$), thus coming very close to the rms value for the rest of the molecule (23 pm). As a result, the *complete* set of NOE-derived distances can be significantly better fulfilled by the average **MDI**$_{av}$ (rms deviations of 25 pm) than by the two simulations **MDI**^{s2e} and **MDI**^{s1e} separately (rms values of 33 pm each).

iii. MD Simulations of II. The conformational analysis and MD refinement for **II** produced results similar to those found for **I**. All simulations for **II** were performed in vacuo; all parameters were treated as described before for **I**. Starting with minimized structures, MD was run 10 ps for equilibration and 40 ps for analysis. The MD structure (βII-turn) stands in contradiction to the X-ray structure (βI-turn). As for glycopeptide **I**, the same NOEs involving Phe^{5}N*H* are in violation (see Table VII). Two NOEs between Phe^{5}N*H*–Ser^{4}C$_\alpha$*H* and Phe^{5}N*H*–Phe^{5}C$_\alpha$*H* are in agreement with a βII-turn, but five other NOEs disagree with this suggestion: they fit only into a βI-turn.

As for the glycopeptide **I**, the NOE data do not correspond to a static model. Again, the assumption of two conformers in fast equilibrium yields better agreement with the NOE data. Two simulations were performed (with restraint of the side chain χ_1 dihedrals) starting from alternate conformations with a βI-turn or a βII-turn between Ser^4–Phe^5. The resulting structures from averaging over 40 ps of MD were named **MDII**^{v1} and **MDII**^{v2}, respectively. For the first simulation, two NOEs were omitted which could not be satisfied by a βI-turn conformation.

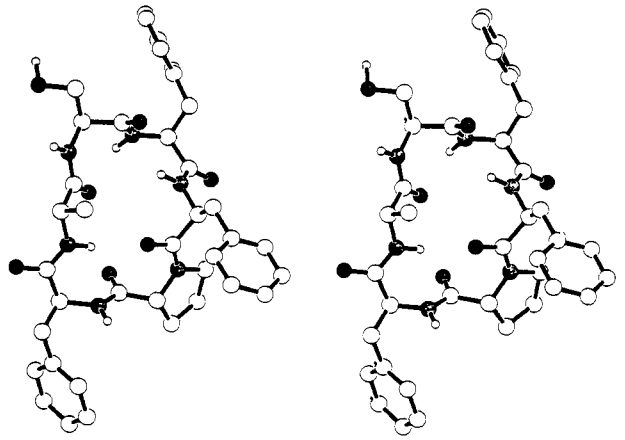

Figure 7. Stereoview of the mean structure of peptide **II** with a βII-turn in the Ala^3 to Phe^6 region, obtained from averaging the 40-ps trajectory from **MDII**^{v2e} (in vacuo) and five steps of restrained energy minimization with the same force constant as applied in the MD simulation. The protons bound to carbon are not shown.

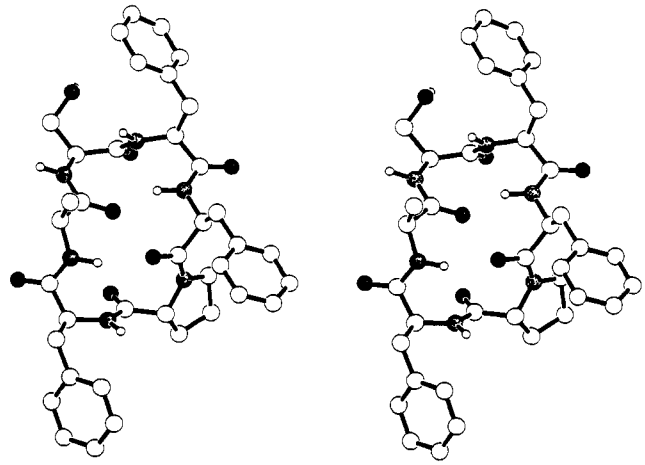

Figure 8. Stereoview of the mean structure of peptide **II** with a βI-turn in the Ala^3 to Phe^6 region, obtained from averaging the 40-ps trajectory from **MDII**^{v1e} (in vacuo) and five steps of restrained energy minimization with the same force constant as applied in the MD simulation. The protons bound to carbon are not shown.

As for **I**, distances were also averaged over both trajectories together under the assumption that both conformations were equally populated (**MDII**$_{av}$). The results for distances and dihedral angles are summarized in Tables VII and IX; the hydrogen bonds are given in the supplementary material.

Again, the distances from **MDII**$_{av}$ show a better agreement with the experimentally derived restraints (rms deviation of 28 pm) than do the simulations **MDII**^{v1} and **MDII**^{v2} (rms values of 35 and 37 pm, respectively). Even more pronounced is the improvement in the Phe^5 region (35 pm for **MDII**$_{av}$, compared to 52 and 56 pm), resulting in a much more uniform agreement over the whole molecule with the NOE data (cf. Table VII).

It should be mentioned that the existing X-ray structure for **II** shows an NOE violation pattern similar to that of the simulations **MDII**^{v1}, i.e., a higher rms value for the distances involving Phe^{5}N*H* than for the rest of the peptide (Table VII), although the crystalline conformation with a βI-turn is almost identical with the average structure **MDII**^{v1}. Obviously, the rigidity of the crystalline βI-turn conformation of **II** contrasts clearly with the requirement of a conformational equilibrium inherent in the NOE data set.

(55) Lautz, J.; Kessler, H.; van Gunsteren, W. F.; Weber, H.-P.; Wenger, R. M. *Biopolymers* **1990**, *29*, 1669–1687.
(56) Hoch, J. C.; Dobson, C. M.; Karplus, M. *Biochemistry* **1985**, *24*, 3831–3841.
(57) Jardetzki, O. *Biochim. Biophys. Acta* **1980**, *621*, 227–232.
(58) Jardetzki, O.; Roberts, G. C. K. *NMR in Molecular Biology*; Academic Press: New York, 1981.

Table VII. Comparison of Experimental and Calculated Proton–Proton Distances for the Cyclic Hexapeptide II[a]

protons		ROESY	MDII[v2]	MDII[v1]	$MDII_{av}$[e]	MDII[tNOE]	X-ray[f]
Phe^5NH	Phe^6NH	239	292	264	278	320	230
Phe^5NH	$Ala^3C_\beta H$	332	532	426	479	505	372
Phe^5NH	$Phe^5C_\alpha H$	218	210	271	241	247	281
Phe^5NH	$Ser^4C_\alpha H$	230	216	347	282	275	349
Phe^5NH	$Ser^4C_\beta H$	284[c]	414	336	375	387	336
Phe^5NH	$Phe^5C_\beta H^{pro\text{-}R}$	299	363	258	311	306	247
Phe^5NH	$Phe^5C_\beta H^{pro\text{-}S}$	347	405	360	383	380	360
$Phe^5C_\alpha H$	$Phe^5C_\beta H^{pro\text{-}S}$	261	244	246	245	242	250
Phe^6NH	$Phe^6C_\alpha H$	270	284	280	282	272	280
Phe^6NH	$Phe^6C_\beta H^{pro\text{-}S}$	285	260	284	272	279	301
Phe^6NH	$Phe^6C_\beta H^{pro\text{-}R}$	296	300	330	315	304	332
$Phe^6C_\alpha H$	$Phe^6C_\beta H^{pro\text{-}S}$	252	287	288	287	287	291
$Phe^6C_\alpha H$	$Phe^6C_\beta H^{pro\text{-}R}$	237	234	236	235	235	246
$Phe^6C_\alpha H$	$D\text{-}Pro^1C_\delta H$	224[c]	221	223	222	224	235
Phe^2NH	Ala^3NH	250	308	286	297	350	253
Phe^2NH	$Phe^2C_\alpha H$	274	278	268	273	274	281
Phe^2NH	$D\text{-}Pro^1C_\alpha H$	207	212	208	210	228	209
Phe^2NH	$Phe^2C_\beta H^{pro\text{-}R}$	258	243	245	244	250	237
Phe^2NH	$Phe^2C_\beta H^{pro\text{-}S}$	331	350	346	348	353	355
$Phe^2C_\alpha H$	$Phe^2C_\beta H^{pro\text{-}S}$	235	241	244	243	241	248
Ala^3NH	$Ala^3C_\alpha H$	272	280	284	282	269	286
Ala^3NH	$Phe^2C_\alpha H$	278	285	328	307	292	317
Ala^3NH	$Ala^3C_\beta H$	255[b]	305	293	299	297	284
$Ala^3C_\alpha H$	$Ala^3C_\beta H$	222[b]	241	240	241	240	236
Ser^4NH	Phe^5NH	316	405	340	372	353	279
Ser^4NH	$Ser^4C_\alpha H$	269	268	249	259	252	276
Ser^4NH	$Ser^4C_\beta H$	260[c]	279	265	272	307	240
Ser^4NH	$Ala^3C_\beta H$	257[b]	309	344	326	345	288
Ser^4NH	$Ala^3C_\alpha H$	236	256	234	245	265	271
Ser^4NH	Ser^4OH	297	363	385	374	355	432
$Ser^4C_\alpha H$	Ser^4OH	277	306	322	314	321	309
			rms Deviations (pm)				
NOEs involving Phe^5NH (1–7)			56	52	35	48 (41)[g]	55
all other NOEs (8–31)			29	27	26	29 (27)[g]	35
complete set of NOEs (1–31)			37	35	28	34 (31)[g]	40

[a] All values are given in pm. For the notation of the different MD trajectories, see text. [b] Increased by 100 ppm for MD run (CH_3 group[36b]). [c] Increased by 90 pm for MD run (CH_2 without diastereotopic assignment[36b]). [d] ROEs omitted in the MD run MDI[v1e] (see text). [e] $MDII_{av}$ indicates averaging over both trajectories MDII[v1] and MDII[v2]. [f] Calculated distances for the solid-state structure of II. [g] Derived from a longer MD trajectory (360 ps).

iv. MD Simulation with Time-Dependent Distance Constraints. As shown above, a single structure cannot account for all of the experimental data. This finding is not too surprising considering that conformational mobility has been observed for similar peptides.[6d] However, recently an approach specially designed for such cases has been proposed.[59] This modified molecular dynamics procedure does not treat the distance restraints as static, but only requires that the distance constraints are satisfied as a $\langle r^{-3}\rangle^{-1/3}$ time-weighed average over the simulated trajectory. This should give a better approximation of the physical nature of the NOEs and, therefore, of the proposed conformational equilibrium.[59]

This technique was applied to refine the structures of compounds I and II with a βII-turn between Ser^4 and Phe^5. For these MD simulations, the initial value of each distance restraint was set to 20 pm less than the experimentally determined distance. The time constant for the decay of the "memory function" was set to 2.5 ps; the rate of motion during the simulation and the required time for the structural refinement are directly affected by this value.[59b] After an initial 10 ps for equilibrating the system without time-dependent distance restraints, 90 ps of in vacuo MD were carried out with K_{dc} = 2000 kJ mol^{-1} nm^{-2} for I (MDI[tNOE]) and II (MDII[tNOE]).

For I the distances (Table VI) and dihedral angles (Table VIII) were calculated as an average over the MD run with time-dependent restraints. The rms deviation (over 37 NOEs) for this simulation is smaller (26 pm) than for the simulations with static distance restraints (33 pm for MDI[s2e] and MDI[s1e]) and is comparable to the distance restraints violation calculated for an averaging between the βII- and βI-turns (25 pm) (cf. Table VI).

The situation is similar with peptide II: the rms deviation of 31 pm over all 31 distances indicates a good approximation of motional averaging with the time-dependent distance constraints (cf. Table VIII). It is in the same range as when averaging over both trajectories MDII[v1] and MDII[v2] together takes place (rms value 28 pm); in both cases, the improvement over the separate MD runs MDII[v1] and MDII[v2] is almost exclusively gained from the distances involving Phe^5NH. In contrast to I, the simulation with the time-dependent restraints needed a longer period of time (360 ps) to lead to a significant reduction in NOE violations; a shorter MD run of 90-ps duration yielded only a slight improvement (Table VII).

In both cases the calculated proton–proton distances with the time-dependent restraints agree with experimentally derived values better than with the single MD runs with either βI- or βII-type turns. The NOEs involving Phe^5NH are better represented during the time scale of the simulation because of the greater flexibility allowed. Hence, the treatment of the NOEs as fixed distance bounds is not correct for these molecules. In Figure 9 (top) the distance between Phe^5NH and $Phe^5C_\alpha H$ (experimental 241 pm) is displayed as a function of time (upper left) during the refinement of I using time-dependent distances. In this trajectory, the NOE restraint was much better satisfied than in the simulations without time-dependent distance restraints. From this plot it is obvious that the NOE bound is violated for several picoseconds during the time span, but for other periods it is satisfied. The transient violation of some other NOEs is reflected here, allowing this NOE to be satisfied and the experimental data to be fulfilled. Figure 9 (upper right) gives an additional view of this result by considering the value of the corresponding NOE calculated with the memory function during the simulation as suggested from ref 59a. This

(59) (a) Torda, A. E.; Scheek, R. M.; van Gunsteren, W. F. *Chem. Phys. Lett.* **1989**, *157*, 289–294. (b) Torda, A. E.; Scheek, R. M.; van Gunsteren, W. F. *J. Mol. Biol.* **1990**, *214*, 223–235.

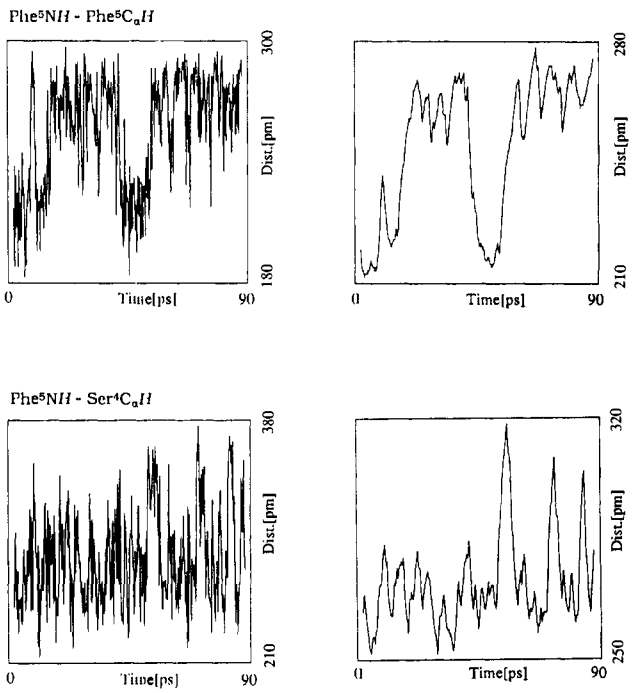

Figure 9. Interatomic distances as a function of time during 90-ps MD simulation of glycopeptide **I** (**MDI**^{tNOE}) and peptide **II** (**MDII**^{tNOE}). The top plots show the distance between Phe^{5}N*H* and Phe^{5}C$_\alpha$*H* of glycopeptide **I**; the bottom plots show the distance between Phe^{5}N*H* and Ser^{4}C$_\alpha$*H* of peptide **II**. In the left panels, the results from MD simulations with time-dependent distance constraints are given. The plots in the right panels are for the same distance and are obtained from the same trajectory, but they are calculated with the memory function as given in ref 59.

distance value actually determines the size of the applied artificial force. As described by Torda et al.,[59] the running average shows a relatively flat shape in contrast to the instantaneous fluctuations in the distances. A similar analysis is shown for the Phe^{5}N*H* to Ser^{4}C$_\alpha$*H* distance of **II** in Figure 9 (bottom).

From the analysis of the trajectories of **I** and **II**, two major rapidly interconverting conformers for both investigated peptides were observed. An additional illustration of the dynamics of the investigated glycopeptide **II** is given in Figure 10. These distance plots show large fluctuations; the physical nature of these motions is the proposed flip of the central amide bond between Ser^4 and Phe^5 to form two different β-turn structures. This oscillating behavior is obvious from a comparison of the distances between Phe^{5}N*H* and Phe^{5}C$_\beta$*H*$^{pro\text{-}R}$ (on the upper side of the peptide backbone) and between Phe^{5}N*H* and Ser^{4}C$_\alpha$*H* (located on the opposite side). The fluctuations of these distances are coupled, further illustrating the motional averaging for the corresponding systems. It should be mentioned that the time scale and height of energetical barriers cannot be obtained from these simulations because of the application of artificial forces (distance restraints).

The positional rms fluctuations for the heavy atoms (data not given) and the torsion angle rms fluctuations (Table IX) are as expected. The fluctuations are larger with the time-dependent distance restraints, with the exception of the torsion angles in the βII′-turn (D-Pro^1-Phe^2): here the stability is not affected by the amide bond rotation of the β-turn on the counterside of the peptide. For the Ser^4 side chain connecting the disaccharide unit to the peptide backbone, it was not possible to determine an experimental value for the χ_1 dihedral because of overlapping signals in the ECOSY spectrum. Hence this dihedral was not fixed during the simulations. When using time-dependent distance constraints, the rms fluctuations about this dihedral increase by a factor of 2.

3. Discussion

A. Conformation of the Monosaccharide Units in I. The structure of each pyranose ring is in agreement with X-ray diffraction studies of the monosaccharides β-D-galactose[60] and β-D-glucose.[61] The averaged structures obtained here are also in accord with previous MD simulations of glucose.[62] For both saccharide units, we observe a $^4C_1$ chair conformation of the six-membered heterocyclic ring. All substituents are located in equatorial positions, with the exception of the α-glycosidic linkage and the Gal^4 hydroxyl group. The absence of conformational transitions from the initial chair form to the other chair or boat-like conformers is consistent with the interpretation of NMR coupling constants.[63]

The fluctuations of the internal ring dihedral angles are similar to the results of Brady for glucose.[62] The rms deviations of these internal ring dihedrals are nearly uniform among the disaccharide

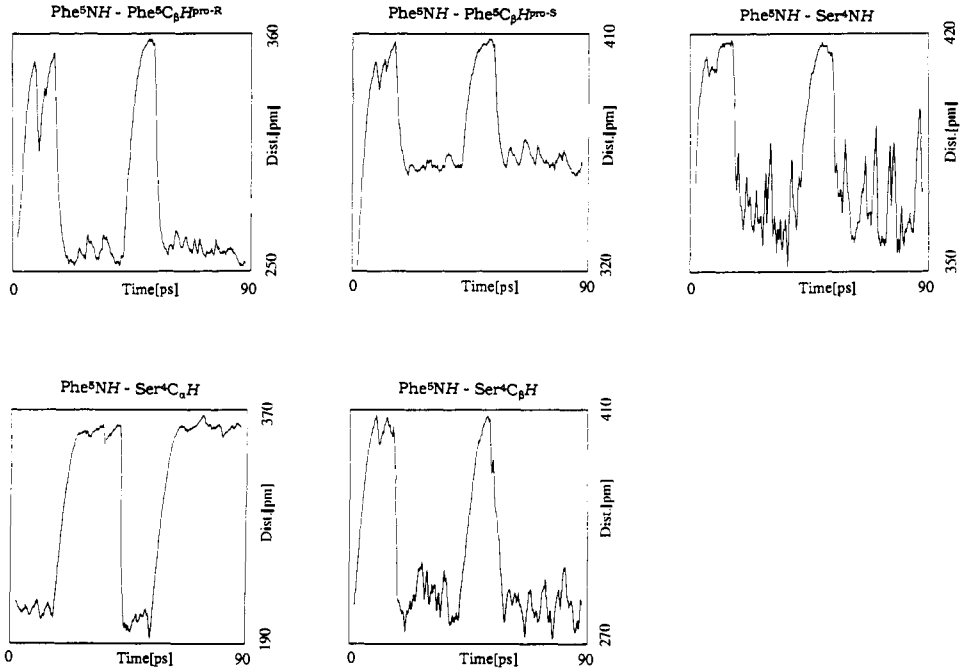

Figure 10. Interatomic distances as a function of time during 90-ps MD simulation of glycopeptide **I** with the application of time-dependent distance constraints. The distances are calculated with the memory function as given in ref 59. The assignment of each plotted distance is given at the top of the corresponding plot.

Table VIII. Comparison of the MD-Calculated Backbone, Side Chain, and Saccharide Dihedrals of Glycopeptide I in Water[a]

		MDI[s2e] βII-turn	MDI[sle] βI-turn	MD[tNOE] dynamic
D-Pro[1]	φ	65.2 (9.5)	63.0 (10.5)	64.7 (12.6)
	ψ	−113.5 (10.8)	−112.4 (14.2)	−110.5 (16.2)
	χ_1	−2.7 (25.3)	−2.4 (26.2)	−4.4 (25.4)
	ω	−177.9 (5.7)	178.7 (5.3)	−179.5 (7.3)
Phe[2]	φ	−70.8 (10.5)	−67.1 (11.4)	−81.8 (20.4)
	ψ	−39.1 (10.3)	−28.6 (15.1)	−14.7 (27.0)
	χ_1	−75.1 (16.2)	−70.6 (12.4)	−60.1 (1.1)[b]
	ω	175.0 (6.2)	169.0 (6.2)	171.3 (11.3)
Ala[3]	φ	−85.4 (12.9)	−96.4 (15.7)	−105.1 (26.5)
	ψ	152.5 (11.4)	157.7 (12.3)	147.3 (40.5)
	ω	177.8 (8.0)	−176.0 (7.9)	176.1 (14.3)
Ser[4]	φ	−64.6 (13.0)	−49.8 (16.9)	−37.9 (41.8)
	ψ	**124.8 (6.9)**	**−68.5 (13.5)**	**−125.7 (96.6)**
	χ_1	−53.9 (7.1)	−59.7 (8.0)	−55.8 (16.0)
	ω	−166.9 (7.8)	172.5 (8.0)	173.4 (11.9)
Phe[5]	φ	**87.4 (11.0)**	**−59.1 (12.5)**	**−11.2 (83.7)**
	ψ	−29.4 (25.1)	−25.3 (20.8)	−20.5 (39.6)
	χ_1	−70.8 (12.8)	−77.5 (22.4)	−60.1 (1.4)[b]
	ω	−179.6 (6.9)	−177.1 (8.3)	179.3 (10.3)
Phe[6]	φ	−134.7 (20.2)	−137.8 (16.8)	−145.5 (36.3)
	ψ	100.9 (16.0)	103.6 (16.1)	109.7 (16.2)
	χ_1	−134.2 (48.0)	−163.5 (13.9)	−179.7 (1.5)[b]
	ω	172.1 (7.0)	170.8 (7.5)	170.2 (9.3)
glycosidic bonds	$O^{5'}$–$C^{1'}$–O^4–C^4	−58.7 (10.5)	−150.7 (32.2)	−98.3 (49.8)
	$C^{2'}$–$C^{1'}$–O^4–C^4	177.1 (9.0)	85.7 (33.3)	139.8 (48.9)
	C^3–C^3–O^4–$C^{1'}$	103.3 (9.2)	72.6 (17.1)	89.5 (41.7)
	O^5–C^1–O^1–Ser$^4C_\beta$	60.1 (9.2)	55.2 (14.0)	60.2 (17.2)
	C^2–C^1–O^1–Ser$^4C_\beta$	−169.6 (7.2)	−174.9 (10.9)	−168.6 (14.7)
D-Glc	O^5–C^1–C^2–C^3	59.0 (5.7)	61.3 (5.9)	56.3 (19.3)
	C^1–C^2–C^3–C^4	−60.6 (5.6)	−58.0 (8.5)	−43.7 (35.1)
	C^1–C^2–C^3–O^3	172.4 (8.2)	178.2 (10.7)	−166.3 (36.6)
	C^2–C^3–C^4–C^5	53.8 (8.2)	44.0 (10.2)	27.2 (37.6)
	C^2–C^3–C^4–O^4	177.9 (6.6)	165.1 (12.0)	146.4 (37.6)
	C^2–C^1–O^5–C^5	−62.5 (5.6)	−62.7 (7.0)	−62.4 (8.8)
	C^1–O^5–C^5–C^4	61.0 (6.7)	54.2 (8.4)	48.9 (13.7)
	C^4–C^5–C^6–O^6	37.6 (96.9)	5.8 (46.5)	−118.7 (396.5)
	C^6–C^5–C^4–C^3	−173.5 (8.3)	−164.4 (9.7)	−150.5 (26.7)
Gal	O^4–$C^{1'}$–$C^{2'}$–$C^{3'}$	−175.0 (8.1)	176.1 (7.8)	169.2 (15.6)
	$O^{5'}$–$C^{1'}$–$C^{2'}$–$C^{3'}$	51.1 (8.1)	54.2 (7.0)	49.4 (14.9)
	$O^{5'}$–$C^{1'}$–$C^{2'}$–$O^{2'}$	172.9 (10.4)	174.8 (8.9)	167.7 (16.1)
	$C1'$–$C^{2'}$–$C^{3'}$–$C^{4'}$	−53.5 (6.9)	−54.6 (8.0)	−52.1 (8.5)
	$C^{1'}$–$C^{2'}$–$C^{3'}$–$O^{3'}$	−176.7 (7.8)	−177.2 (9.4)	−174.3 (10.1)
	$C^{2'}$–$C^{3'}$–$C^{4'}$–$C^{5'}$	58.3 (6.9)	55.5 (6.7)	56.0 (6.1)
	$C^{2'}$–$C^{3'}$–$C^{4'}$–$C^{5'}$	58.3 (6.9)	55.5 (6.7)	56.0 (6.1)
	$C^{2'}$–$C^{3'}$–$C^{4'}$–$O^{4'}$	−65.3 (7.7)	−71.4 (9.5)	−67.0 (7.4)
	$C^{2'}$–$C^{1'}$–$O^{5'}$–$C^{5'}$	−57.2 (6.9)	−59.9 (7.5)	56.0 (6.1)
	$C^{1'}$–$O^{5'}$–$C^{5'}$–$C^{4'}$	62.3 (5.6)	61.1 (8.3)	59.3 (15.4)
	$C^{4'}$–$C^{5'}$–$C^{6'}$–$O^{6'}$	−66.9 (80.7)	0.4 (99.7)	−153.4 (353.6)
	$C^{6'}$–$C^{5'}$–$C^{4'}$–$C^{3'}$	174.0 (7.4)	176.5 (7.6)	177.8 (7.6)

[a] All angles are given in degrees; the numbers in parentheses denote the rms fluctuation obtained by averaging. Values indicating the peptide bond flip are shown in boldface type. [b] Side chain χ_1 dihedral angle fixed by additional torsion angle potential according to NMR results.

residues, with typical values for fluctuation of 5–10° (with the exception of the simulation with time-dependent distance constraints). These data are consistent with β-D-glucose force field calculations, suggesting that monosaccharide residues may undergo changes in ring conformations of up to 10° in dihedral angles.[64]

B. Conformation of the Glycosidic Bonds. i. β(1–4)-Glycosidic Linkage. In disaccharides, the exoanomeric effect does not change the conformation which would be adopted because of steric interactions alone. This effect only narrows the potential well and becomes more important in the case of complex oligosaccharides, where steric factors are less favorable.[65]

A comparison of the β-glycosidic torsion angles obtained by X-ray diffraction of α-lactose[66] or β-cellobiose[67] reveals a great correspondence in molecular shape. This comparison naturally suffers from the lack of the hydroxyl substituent at Glc-C^2 in the investigated glycopeptide. The averaged dihedral angles from the MD simulations in water, in DMSO, and in vacuo about this β(1–4)-glycosidic bridge are given in Tables VIII and X. The φ angle is −92.6° (φ_2 = 94.6°, C^2–C^2–O^1–$C^{4'}$) and −77.8° (φ_2 = 106.0°) in α-lactose[66] and β-cellobiose,[67b] respectively. For a fully extended conformation, these angles are expected to adopt values of φ = −110° and φ_2 = +110°. Lactose exhibits a symmetrical twist around the glycosidic bond, whereas cellobiose exhibits an asymmetrical twist. This modification of the fully extended conformation for the β-glycosidic bond is assumed to be a consequence from an interresidual hydrogen bond from O^3–H···$O^{5'}$.

(60) Longchambon, P. F.; Ohannessian, J.; Avenel, D.; Neuman, A. *Acta Crystallogr.* **1975**, *B31*, 2623–2627.
(61) Arnold, S.; Scott, W. E. *J. Chem. Soc., Perkin Trans. 2* **1972**, 324–335.
(62) (a) Brady, J. W. *J. Am. Chem. Soc.* **1986**, *108*, 8153–8160. (b) Brady, J. W. *J. Am. Chem. Soc.* **1989**, *111*, 5155–5165.
(63) Kottenhahn, M. Ph.D. Thesis, Frankfurt FRG, 1989.
(64) Rao, V. S. R.; Joshi, N. V. *Biopolymers* **1979**, *18*, 2993–3004.
(65) Lemieux, R. U.; Wong, T. C.; Thøgersen, H. *Can. J. Chem.* **1982**, *60*, 81–86.
(66) Fries, D. C.; Rao, S. T.; Sundaralingam, M. *Acta Crystallogr.* **1971**, *B27*, 994–1005.
(67) (a) Jacobsen, R. A.; Wunderlich, J. A.; Libscomb, W. N. *Acta Crystallogr.* **1961**, *14*, 598–607. (b) Chu, S.; Jeffrey, G. A. *Acta Crystallogr.* **1968**, *B24*, 830–838.

Table IX. Comparison of the Experimental (X-ray Analysis) and MD-Calculated Backbone and Side Chain Dihedrals of the Cyclic Hexapeptide II[a]

		MDII^{v2} βII-turn	MDII^{v1} βI-turn	MDII^{tNOE} dynamic	X-ray βI-turn
D-Pro^1	φ	60.4 (9.9)	59.6 (10.6)	69.3 (14.6)	65.9 (9)
	ψ	−124.6 (14.7)	−112.8 (12.1)	−92.0 (38.5)	−135.4 (7)
	χ_1	−9.0 (23.7)	3.8 (25.6)	−5.3 (26.0)	−1.0 (1)
	ω	177.5 (6.3)	179.2 (6.3)	175.6 (10.2)	175.1 (6)
Phe^2	φ	−86.4 (18.1)	−65.5 (17.5)	−83.2 (32.8)	−88.9 (8)
	ψ	22.2 (37.2)	−21.6 (29.4)	−73.9 (99.0)	1.0 (1)
	χ_1	−60.0 (1.6)	−60.0 (1.5)	−60.0 (2.2)	−71.2 (8)
	ω	−179.4 (9.5)	173.6 (8.9)	179.4 (11.3)	178.4 (7)
Ala^3	φ	−130.8 (34.0)	−110.5 (27.3)	−97.4 (70.2)	−91.9 (8)
	ψ	175.7 (15.9)	148.1 (20.1)	−174.5 (91.7)	−176.8 (6)
	ω	172.1 (8.6)	−177.9 (9.0)	179.1 (12.5)	−173.7 (6)
Ser^4	φ	−59.9 (11.9)	−27.3 (25.9)	−25.2 (66.3)	−65.3 (8)
	ψ	**98.0 (10.9)**	**−51.2 (18.1)**	**19.7 (68.2)**	**−38.5 (9)**
	χ_1	−88.5 (48.1)	125.9 (61.9)	−22.1 (230.9)	−177.0 (6)
	ω	174.9 (6.4)	177.9 (6.0)	179.3 (10.1)	−172.0 (6)
Phe^5	φ	**86.7 (16.7)**	**−89.9 (29.9)**	**163.8 (95.5)**	**−104.5 (7)**
	ψ	−26.2 (27.8)	−20.4 (31.8)	156.8 (226.8)	−12.5 (9)
	χ_1	−60.2 (1.7)	−59.9 (1.7)	−60.4 (2.2)	−66.0 (8)
	ω	179.5 (8.8)	−177.7 (7.8)	178.8 (11.3)	−171.4 (6)
Phe^6	φ	−114.0 (25.4)	−144.5 (18.9)	34.8 (262.3)	−163.3 (6)
	ψ	109.3 (15.2)	106.2 (15.5)	105.9 (20.1)	143.2 (6)
	χ_1	−179.8 (1.0)	−180.0 (1.8)	−179.6 (2.1)	−172.3 (6)
	ω	176.2 (8.6)	173.7 (7.2)	−176.8 (12.8)	172.7 (6)

[a] All angles are given in degrees; the numbers in parentheses denote the rms fluctuation obtained by averaging.

Table X. Comparison of the MD-Calculated Glycosidic Bond Dihedral Angles of the Glycopeptide I[a]

MD simulation	$O^{5'}$–$C^{1'}$–$O^{4'}$–C^4	$C^{2'}$–$C^{1'}$–O^4–C^4	C^3–C^4–O^4–$C^{1'}$	O^5–C^1–O^1–Ser$^4C_\beta$	C^2–C^1–O^1–Ser$^4C_\beta$
(1) Simulation in Water with Exoanomeric Effect Potential					
MDI^{s2e} (βII)	−58.7	177.1	103.3	60.1	−169.6
MDI^{s1e} (βI)	−150.7	85.7	72.6	55.2	−174.9
(2) Simulation in Water without Exoanomeric Effect Potential					
MDI^{s2} (βII)	−68.5	169.6	106.1	75.3	−156.9
MDI^{s1} (βI)	−65.3	172.5	103.3	75.6	−154.0
(3) Simulation in Vacuo (Reduced Charges) with Exoanomeric Effect Potential					
MDI^{v2e} (βII)	−79.0	158.1	156.2	48.9	179.2
MDI^{v1e} (βI)	−116.6	122.5	93.2	31.7	162.8
MDI^{tNOE}	−98.3	139.8	89.5	60.2	−168.6
(4) Simulation in Vacuo (Reduced Charges) without Exoanomeric Effect Potential					
MDI^{v2} (βII)	−90.0	148.5	98.6	109.2	−124.0
MDI^{v1} (βI)	−91.9	146.7	101.2	60.3	−168.6
(5) Simulation in DMSO with Exoanomeric Effect Potential					
MDI^{d2e} (βII)	−62.8	174.5	93.8	63.8	−166.5
MDI^{d1e} (βI)	−77.0	159.7	95.8	42.9	176.5
(6) Starting Structures for Both Turns after Energy Minimization					
EM (βII)	−75.2	163.0	114.7	66.5	−167.0
EM (βI)	−78.1	160.8	109.5	67.2	−164.3
(7) Solid-State Structures for Disaccharides from the Literature					
α-lactose	−92.6	146.2	94.6		
β-cellobiose	−77.8	167.3	106.0		

[a] All angles are given in degrees; they are obtained in each case by averaging over the whole trajectory.

This hydrogen bond was observed in several solid-state structures from β(1–4)-linked oligosaccharides, but could not be detected in the different MD trajectories in water, in DMSO, or in vacuo.

Initial values for these glycosidic dihedrals φ in the glycopeptide I of −75.2° (for βII structure) of −78.1° (for βI structure) were obtained after various energy minimizations. They are close to the values found for β-cellobiose in the solid state. The MD refinements in vacuo without the additional exoanomeric potential produce average dihedral angles of −90.0° (**MDI^{v2}**) and −91.9° (**MDI^{v1}**) for both conformers, which are close to the dihedral values of α-lactose in the solid state. When analyzed, the first set of simulations *in water* without the exoanomeric effect showed a small conformational change (φ values of −68.5° (**MDI^{s2}**) and −65.3° (**MDI^{s1}**)). These values are in the accepted range for values of the β(1–4)-linkage, but they differ by about 30° from the results obtained from in vacuo trajectories. All observed conformations are in agreement with the short deoxyGlcC^4*H*–GalC$^{1'}$*H* distance of 212 pm. In the NOESY spectrum, another NOE between both saccharide moieties (GalC$^{1'}$*H*–deoxyGlcC^6*H*) was observed and was qualitatively in agreement with our results; a quantitative examination of this distance was not possible because of signal overlap. As stated several times in the literature (see, for example, ref 50), only one or two NOEs are available across glycosidic linkages, a situation which complicates oligosaccharide conformational analysis.

The implementation of the exoanomeric effect in the GROMOS force field produces some slightly different results. In vacuo, φ values of −79.0° (for the βII structure) and −116.6° (for the βI structure) were observed. The subsequent simulations in water also show that the different peptide backbone conformers tend to produce different β(1–4)-glycosidic angle conformations: φ values of −58.7° for the βII structure and −150.7° for the βI

structure are observed. Additional MD simulations in water from different starting geometries produced similar results for the glycosidic angles (no data given). This difference in φ of 90° from the analysis of the simulations for the βI/βII conformers could not be checked by experimental methods. The measured short distance between GalC^{1}H and deoxyGlcC^{4}H was only fulfilled for the **MDI**^{s2e} simulation; a violation of 40 pm was observed for the **MDI**^{s1e} simulation, but several theoretical studies revealed a high flexibility around β(1–4)-glycosidic linkages. From the MD simulations in DMSO with the exoanomeric effect, φ values of −77.0° for the βI structure and −62.8° for the βII structure were observed: no alternate conformer or increased flexibility of the glycosidic linkage could be detected during these simulations. In a recent study on the dynamics of several types of glycosidic linkages by molecular dynamic methods, Yan and Bush[68] described three low-energy conformations for β-methyl lactoside (Gal(β-(1–4)Glc-β-O-Me) on the potential energy map. The glycosidic dihedral angles from in vacuo trajectories over 120 ps show these conformations in accord with local minima on the potential energy map. The low-energy conformation with $\varphi = -145.4°$ and $\psi = 99.5°$ corresponds to our alternate conformation around this linkage from the simulation of the βI-turn structure in water.

Not only are the averaged glycosidic dihedral angles different, but the observed flexibility is also greater in the trajectories including the additional parameters for the exoanomeric effect. The results presented here for this linkage are in agreement with the conclusion of an ensemble average over several conformations of these β(1–4)-linked disaccharide fragments.

The high flexibility of the β(1–4)-glycosidic linkage is often discussed in the literature.[68] Dabrowski and co-workers described a dynamical averaging of each of the glycosidic linkages (for Gal-β(1–4)-Glc fragment) during analysis of the conformations of globoside[69] and ganglioside.[70] On the basis of the features of potential energy surfaces as functions of the linkage dihedral angles of cellobiose and maltose, a wider range of allowed conformations for glycosidic linkages is postulated.[71] They are separated by small barriers, leading to the assumption of fast rates of conformational interchange. Therefore NMR reflects only weighted averages, as observed for the peptide backbone. The same results for the occurrence of "alternative" glycosidic linkage conformations and an increased flexibility in those regions were described by Homans.[50] The observations from the MD simulations presented here are consistent with these results. The glycosidic angles for the presented glycopeptide **I** show, in some cases, transitions between distinct conformations.

The modified GROMOS force field now reproduces the theoretical predictions concerning dynamics and flexibility around the β(1–4)-glycosidic linkage significantly better. In vacuo MD simulations on β-lactose as a model compound (data not given) produced other conformations significantly populated around the glycosidic bond only when the modified force field was utilized. These alternate conformations correspond to the low-energy conformers of β-methyl lactoside as described by Yan and Bush.[68]

Obviously the βI/βII-turn dynamics of the peptide backbone influences the geometry of the β(1–4)-glycosidic linkage. Different peptide conformers stabilize different disaccharide conformers or lead to different motional behavior about the glycosidic linkages. However, it is not possible to *experimentally* confirm the conformations about the glycosidic linkage observed in the calculations.

ii. α(1-SerO^{β})glycosidic Linkage. The observed conformations for the α-glycosidic linkage are in agreement with the exoanomeric effect theory. The conformations observed here are also in accord with the reported structures of other linear glycopeptides with Gal-*N*-Ac linked to Thr-O^{β}.[4b,c,i,72] In the literature, these dihedral angles are found to be constrained to a relatively narrow range of values.

The relative geometry of the disaccharide chain to the peptide backbone could be experimentally determined by observation of several NOEs: Ser^{4}N*H*–deoxyGlc*H*^{2eq}, 445 pm (454 pm calculated in **MDI**$^{(NOE)}$); Ser^{4}N*H*–deoxyGlc*H*^{1}, 384 pm (430 pm calculated); Ser^{4}C$_\alpha$*H*–deoxyGlc*H*^{1}, 335 pm (392 pm calculated); and Ser^{4}C$_\beta$*H*–deoxyGlc*H*^{1}, 311 pm (369 pm calculated, increased by 90 pm for MD simulation because of the lack of diastereotopic assignment). These NOEs are fulfilled in all structures; the observed discrepancies (largest violation 57 pm) may arise from an incorrect interpretation of NOE data under the assumption of isotropic mobility in both parts of this molecule or from internal dynamics (torsional oscillations around this linkage).

A detailed examination of the different MD trajectories produced with the different force fields shows that taking the exoanomeric effect into account constrains the $\alpha(1-O^{\beta})$-linkages; no alternate conformations around this linkage appear. This observation is in agreement with theoretical predictions concerning the motional dynamics of this linkage. To summarize the results produced with the modified GROMOS force field, the conformational dynamics and the occurrence of alternate conformers are better reflected by taking the exoanomeric effect into account as proposed by Homans[50] for both types of glycosidic linkages investigated in this report.

The conformation of the primary disaccharide hydroxyl groups, characterized by the torsion angle C^4–C^5–C^6–O^6, changes greatly during all simulations, as reflected by the rms torsion angle fluctuation. A detailed description of preferred conformations about the C^5–C^6 bond was not carried out based on this data set. This observation was also made in MD simulations from several workers,[62,68] whereas the analysis from solid-state structures revealed preferences for this dihedral angle.[66,67]

4. Conclusions

A. Peptide Conformations of I and II. Restrained MD simulations have indicated the high internal flexibility of the cyclic hexapeptide backbone for both **I** and **II**. Two different turn structures could be detected: assuming an ensemble containing both conformers, all NMR data can be accounted for. A great similarity between the corresponding conformers of **I** and **II** was observed (e.g., hydrogen-bond pattern, peptide backbone, and side chain geometry). For both cases it was possible to refine the NMR-derived averaged data by use of a new simulation technique with time-dependent distance constraints, showing both postulated conformers to be in fast equilibrium. This is an illustrative example of a case where the assumption of static structures is not correct; the NOE data set used to derive distance constraints is affected by motional averaging. A refinement to represent all of these experimental data in one single structure would lead to a so-called *virtual structure* without any physical significance, as pointed out previously by Jardetzky.[57] These kind of structures derived from NMR remain poorly defined despite the availability of NMR parameters of high quality.[73]

The βI conformer of **II** corresponds to the solid-state structure of **II** with some small differences in dihedral angles (Table IV), but with no major change in molecular shape. This leads to the assumption of an increased stability of βI-turns in crystal environments, probably because of intermolecular packing effects. The preference of βI-turns in an L,L-amino acid sequence has long been referred to in the literature.[74] The results presented here reveal the flexibility in those turns in solution. Comparison of the molecular mobility during MD refinements of **I** and **II** shows that

(68) Yan, Z.-Y.; Bush, C. A. *Biopolymers* **1990**, *29*, 799–811.
(69) Poppe, L.; von der Lieth, C.-W.; Dabrowski, J. *J. Am. Chem. Soc.* **1990**, *112*, 7762–7771.
(70) Acquotti, D.; Poppe, L.; Dabrowski, J.; von der Lieth, C.-W.; Sonnino, S.; Tettamanti, G. *J. Am. Chem. Soc.* **1990**, 7772–7778.
(71) Stevens, E. S.; Sathyanarayana, B. K. *J. Am. Chem. Soc.* **1989**, *111*, 4149–4154.
(72) Ferrari, B.; Pavia, A. A. *Int. J. Pept. Protein Res.* **1983**, *22*, 549–559.
(73) (a) Scarsdale, J. N.; Yu, R. K.; Prestegard, J. H. *J. Am. Chem. Soc.* **1986**, *108*, 6778–6784. (b) Kim, Y.; Ohlrogge, J. B.; Prestegard, J. H. *Biochem. Pharmacol.* **1990**, *40*, 7–13. (c) Holak, T. A.; Keasely, S. K.; Kim, Y.; Prestegard, J. H. *Biochemistry* **1988**, *27*, 6135–6142.
(74) (a) Venkatachalam, C. M. *Biopolymers* **1968**, *6*, 1425–1436. (b) Lewis, P. N.; Momany, F. A.; Scheraga, H. A. *Biochim. Biophys. Acta* **1973**, *303*, 211–229. (c) Némethy, G.; Scheraga, H. A. *Biochem. Biophys. Res. Commun.* **1980**, *95*, 320–327.

both compounds reveal corresponding flexibilities. Furthermore, no significant effect of the oligosaccharide chain on the peptide backbone mobility was observed. This is different from results indicating the stiffening of a peptide chain containing glycosylated amino acid residues (for example, see ref 4e).

The results presented here show that both peptides have similar conformations and dynamics in solution. The O-glycosylation does not change the overall shape of the investigated peptide. The glycosylation has no significant influence on the population of side chain rotamers in the neighborhood of the glycosylated amino acid. A fast interconversion between two significantly populated conformers (differing by the type of β-turn in equilibrium) could be detected for both peptides. Simulations with time-dependent distance constraints for both peptides led to further evidence on the proposed interconversion.

B. Conformation of the Monosaccharide in I. The analysis of the MD simulations suggests that the peptide backbone conformation obviously influences the relative geometry of the β(1–4)-glycosidic linkage or the conformational averaging around this linkage. The in vacuo and in water simulations with a potential taking into account the exoanomeric effect produce a significant population of an alternative conformer around the β(1–4)-glycosidic linkage when the peptide backbone changes from βI to βII. While all obtained conformations for both peptides could be verified by several measured distances, the situation for the determination of the oligosaccharide spatial structure critically depends on the nature of the employed force field because of the lack of NOEs between the monosaccharide subunits. The simulations including the exoanomeric effect show better agreement with results from calculations of other workers in respect to the average glycosidic dihedral angles; higher flexibility leading to conformational averaging around the β(1–4) bond as observed in our MD simulations has also been proposed several times by other groups using independent methods. In fact, it is difficult to decide whether the modified parametrization (including the exoanomeric effect) will lead to a physically more realistic picture of the motional behavior of glycosidic linkages because of the lack of experimental data yielding insight into the conformational distributions around these bonds.

5. Experimental Section

A. X-ray Structure Determination of Cyclo(D-Pro-Phe-Ala-Ser-Phe-Phe)·3DMSO. Colorless transparent crystals were obtained from a saturated solution of the hexapeptide in DMSO. A crystal with dimensions 0.39 × 0.50 × 0.50 mm was sealed in a glass capillary together with a drop of mother liquor. The measurements were performed on an Enraf-Nonius CAD4 diffractometer with Cu Kα radiation (graphite monochromator) at room temperature (294 K). Crystal data: $C_{38}H_{44}N_6O_7 \cdot 3C_2H_6SO$, monoclinic space group $P2$ (No. 4), a = 10.099 (2), b = 10.403 (1), c = 23.276 (2) Å, β = 92.24 (1)°, V = 2443.4 (8) Å^3, Z = 2, ρ_{calc} = 1.269 g/cm^3, μ = 18.4 cm^{-1}. A total of 6673 reflections in the $\pm h,+k,\pm l$ hemisphere were measured up to 2θ = 108° using an ω-scan with $\Delta\omega$ = 1.8° + 0.21° tan θ. Three standard reflections remeasured every 5500 s remained stable. An empirical absorption correction was made based on the psi scans of five reflections.[75] The correction factor ranged from 1.00 to 1.39. Equivalent reflections were averaged ($R(F)$internal = 0.046), resulting in 3125 unique reflections with $I > 0$, which were used for the structure determination and refinement.

The structure was determined by Patterson search techniques using the program PATSEE.[76] A fragment containing 29 atoms taken from the crystal structure of cyclo(D-Pro-Phe-Phe-Pro-Phe-Phe)[13] was earlier positioned and subsequently expanded to the full structure by tangent refinement. The hydrogen position of the Ser^{4}OH group was derived from a difference Fourier synthesis. All other H-atoms of the main molecule were placed at idealized calculated positions. The H-atoms at the poorly ordered DMSO molecules could not be determined. The H-atoms were not varied. The C-atoms of DMSO were refined with isotropic thermal parameters. All other non-H-atoms were refined with anisotropic thermal parameters. The structure refinement of the F values using unit weights converged at $R(F)$ = 0.067 and $\omega R(F)$ = 0.067.

The final difference Fourier synthesis showed residual density up to 1.0 e/Å^3 near the S-atoms of the disordered DMSO molecules, but was otherwise featureless. The positional and anisotropic thermal parameters are reported in Tables S1 and S2, while Tables S3–S6 contain bond distances, bond angles, torsion angles, and structure factor listings; all are included in the supplementary material. The calculations were performed with the SDP program system.[77]

B. NMR Measurements. The spectra were recorded on Bruker spectrometers: AMX 600, AMX 500, and AC 250. The samples contained 30 and 20 mg of I and II, respectively, in 0.5 mL of DMSO-d_6 (99.9% ^{2}H-atoms; Aldrich). All chemical shifts are referenced to the DMSO-d_6 signal at 2.5 ppm for ^{1}H and 39.5 ppm for ^{13}C.

i. 1D ^{1}H NMR Spectra. Size 16K, pulse length 3.0 μs, 80 acquisitions. The spectra for determination of the temperature gradients were recorded at 300–340 K in steps of 10 K for I and II.

ii. DQF-COSY Spectra. Sequence: D_1–90°–t_1–90°–D_2–90°–t_2. Relaxation delay D_1 = 1.3 s, D_2 = 4 μs, 90° pulse 7.8 μs. Spectral widths in both dimensions f_1 and f_2 were 7142.8 Hz for 600 MHz and 2994.0 Hz for 250 MHz, with quadrature detection in both dimensions.

iii. NOESY Spectrum. Sequence: D_1–90°–t_1–90°–τ_{mix}–90°–t_2. Relaxation delay, D_1 = 1.3 s; mixing time (τ_{mix}), 100 ms, no random variation of τ_{mix}; 90° pulse 7.8 μs. Spectral width in both dimensions f_1 and f_2 was 7142.8 Hz, with quadrature detection in both dimensions.

iv. TOCSY Spectra. Sequence: D_1–90°–t_1–MLEV17–t_2. Relaxation delay, D_1 = 1.3 s; spectra with different mixing times (duration of the spin-lock period) were recorded (a, 20 ms; b, 80 ms), 90° pulse 7.8 μs. Spectral widths in both dimensions f_1 and f_2 were 7142.8 Hz for 600 MHz and 2994.0 Hz for 250 MHz, with quadrature detection in both dimensions.

v. ROESY Spectrum for II. Sequence: D_1–90°–t_1–$(P_5$–$D_3)_n$–t_2. Relaxation delay, D_1 = 1.3 s, D_3 = 20.5 μs, 90° pulse 7.8 μs, P_5 pulse for spin-lock field 2 μs, mixing time 150 μs. Spectral width in both dimensions f_1 and f_2 was 2994.0 Hz, with quadrature detection in both dimensions.

vi. ECOSY Spectra. Sequence: D_1–90°–t_1–90°–D_2–90°–t_2. Relaxation delay, D_1 = 1.3 s, D_2 = 3 μs, 90° pulse 7.1 μs. Spectral width in both dimensions f_1 and f_2 was 2000.0 Hz, with quadrature detection in both dimensions.

vii. Proton-Detected Heteronuclear Correlation (HMQC) Spectra. Sequence: D_1–BIRD–D_4–90°(^{1}H)–D_2–90°(^{13}C)–$t_1/2$–180°(^{1}H)–$t_1/2$–90°(^{13}C)–D_2–t_2(GARP[^{13}C]). Relaxation delay, D_1 = 197 ms, D_2 = 3.57 ms, D_4 = 117 ms, 90° pulse (^{1}H) 12.5 μs, 90° pulse (^{13}C) 10.4 μs. Spectral width in f_2 was 5434.78 Hz (=9.056 ppm) and f_1 was 11 363.64 Hz (=75.3 ppm), with quadrature detection in both dimensions, recording and processing in the pure absorption mode.

viii. "Inverse COLOC" with 270° Gaussian Pulse (HMBCS-270) Spectra. Sequence: D_1–90°(^{1}H)–D_4–270°$_{selective}$(^{13}C)–$t_1/2$–180°(^{1}H)–$t_1/2$–90°(^{13}C)–t_2. Relaxation delay, D_1 = 2.0 s, 90° pulse (^{1}H) 7.8 μs, 90° pulse (^{13}C hard) 12.4 μs, 270° pulse (^{13}C soft) 2000 μs, D_4 = 50 ms. Spectral width in f_2 was 5555.56 Hz, in f_1, 140.0 Hz. The spectra were recorded and processed in the phase-sensitive mode, followed by a magnitude calculation in f_2.

ix. Proton-Detected Heteronuclear Correlation with TOCSY Transfer (HMQC-TOCSY) Spectra. Sequence: D_1–BIRD–D_4–90°(^{1}H)–D_2–90°(^{13}C)–$t_1/2$–180°(^{1}H)–$t_1/2$–90°(^{13}C)–D_2–MLEV17–t_2(GARP[^{13}C]). Relaxation delay, D_1 = 197 ms, D_2 = 3.57 ms, D_4 = 117 ms, 90° pulse (^{1}H) 12.5 μs, 90° pulse (^{13}C) 10.4 μs. Spectral width in f_2 was 5434.78 Hz (=9.056 ppm) and in f_1, 11 363.64 Hz (=75.3 ppm); mixing time for the spin-lock was 80 ms, with quadrature detection in both dimensions and recording and processing in the pure absorption mode.

x. HMQC-NOESY Spectrum for I (600 MHz). Sequence: D_1–BIRD–D_4–90°(^{1}H)–D_2–90°(^{13}C)–$t_1/2$–180°(^{1}H)–$t_1/2$–90°(^{13}C)–D_2–90°(^{1}H)–τ_{mix}–90°(^{1}H)–t_2(GARP[^{13}C]). Relaxation delay, D_1 = 235 ms, D_2 = 3.57 ms, D_4 = 225 ms, 90° pulse (^{1}H) 12.5 μs, 90° pulse (^{13}C) 10.4 μs. Spectral width in f_2 was 5434.78 Hz (=9.056 ppm) and in f_1, 11 363.64 Hz (=75.3 ppm); mixing time for the NOE transfer step was 200 ms, with quadrature detection in both dimensions and recording and processing in the phase-sensitive mode. Co-added rows of a spectral region without cross-peaks were subtracted from the 2D matrix.

Acknowledgment. Financial support by the Deutsche Forschungsgemeinschaft and the Fonds der Chemischen Industrie is gratefully acknowledged. We thank Prof. Dr. W. F. van Gunsteren and Dr. A. E. Torda for the GROMOS package and helpful discussions and Dr. D. F. Mierke for his careful reading

(75) North, A. C. T.; Phillips, D. C.; Mathews, F. S. *Acta Crystallogr. Sect. A* **1968**, *24*, 351–359.
(76) Egert, E.; Sheldrick, G. M. *Acta Crystallogr. Sect. A* **1985**, *41*, 262–268.
(77) Structure Determination Package, Enraf-Nonius, Delft, The Netherlands, 1986.

of the manuscript. M.K. and H.M. thank the Fonds der Chemischen Industrie for a fellowship.

Supplementary Material Available: Tables S1-S5 containing positional and anisotropic thermal parameters, bond distances and angles, and torsion angles from the X-ray structure of II, Tables S7-S10 containing atomic coordinates of averaged MD structures of I from water simulations and II from in vacuo calculations, Tables S11-S13 containing calculated distances, dihedral angles, and hydrogen bonds from MD simulations of I in DMSO, and Tables S14 and S15 containing hydrogen bonds from different MD simulations of I (in water) and II (in vacuo) (20 pages); Table S6 containing observed and calculated structure factors (28 pages). Ordering information is given on any current masthead page.

Conformation of Cyclic Analogues of Substance P: NMR and Molecular Dynamics in Dimethyl Sulfoxide

Juris Saulitis,[‡] Dale F. Mierke, Gerardo Byk,[†] Chaim Gilon,[†] and Horst Kessler*

Contribution from the Organisch Chemisches Institut, Technische Universität München, Lichtenbergstrasse 4, 8046 Garching, Germany, and Department of Organic Chemistry, Hebrew University of Jerusalem, Jerusalem 91904, Israel. *Received May 20, 1991*

Abstract: The conformational analysis of two cyclic analogues of substance P has been carried out using NMR spectroscopy and restrained molecular dynamics calculations. The cyclic analogues, cyclo[-$(CH_2)_m$-NH-CO-$(CH_2)_n$-CO-Arg-Phe-Phe-N-]-CH_2-CO-Leu-Met-NH_2 (with m, n = 3, 2 and 3, 3), show a large percentage of cis configurational isomers (18 and 22%) about the substituted amide. The additional isomers lead to severe spectral overlap of the proton resonances. Using the carbon resonances and the associated large chemical shift dispersion allows for the unambiguous assignment of all proton resonances. From the NOEs, temperature gradients, and coupling constants the conformation of the cyclic portion of the molecule is well-determined. The structures obtained from the experimental study were refined with NOE-restrained molecular dynamics. The computer simulations were carried out in dimethyl sulfoxide, the same solvent used in the experimental study. The dynamic stability of the refined conformations was evaluated by performing an extended, free MD simulation (400 ps) in dimethyl sulfoxide. The comparison of the interproton distances from the NOEs (two-spin approximation) with the effective distances from the free MD simulation is introduced as a possible tool to test the quality of obtained structures.

Introduction

Substance P (SP) is an undecapeptide, Arg-Pro-Lys-Pro-Gln-Gln-Phe-Phe-Gly-Leu-Met-NH_2, belonging to the tachykinins, a family of peptides sharing the common C-terminal amino acid sequence Phe-Xaa-Gly-Leu-Met-NH_2 and a broad range of biological activities.[1] In fact, the C-terminal hexapeptide of SP, Gln-Phe-Phe-Gly-Leu-Met-NH_2, retains much of the biological activity of the native molecule. The role of SP in the transmission or modulation of pain stimuli is of particular interest.[2] Three different classes of receptors for SP have been identified and cloned (neurokinin receptors NK-1, NK-2, and NK-3).[3] The wide range of physiological activity of SP has been attributed to the lack of selectivity of SP for a particular receptor type. The conformational flexibility of the linear peptide can account for the lack of selectivity.

One method to reduce the conformational freedom of a peptide and greatly increase the selectivity for receptors is cyclization. This method has been applied successfully to many different peptide systems.[4] Therefore, the goals in the cyclization of the neuropeptide substance P were 2-fold. The first goal was to develop a highly selective, metabolically stable analogue. The second goal was to impose conformational constraint in order to lock the peptide in a bioactive conformation that fits each tachykinin receptor.

However, the C-terminal hexapeptide of SP is resistant to cyclization. The common methods for cyclization including end-to-end, end-to-side chain, and side chain-to-side chain lead to analogues with little or no activity.[5] The side chains commonly used for cyclization cannot be modified and, in addition, the C-terminal portion must be free as an amide.

To overcome the limitations of the conventional modes of cyclization, we have recently[6] introduced a new general concept for

* To whom correspondence should be addressed at the Technische Universität München.
‡ Deceased September 9, 1991.
† Hebrew University of Jerusalem.

(1) Pernow, B. *Pharmacol. Rev.* **1983**, *35*, 85-141.
(2) Nicoll, R. A.; Schenker, C.; Leeman, S. E. *Annu. Rev. Neurosci.* **1980**, *3*, 227-268.
(3) (a) *Trends Pharm. Sci. Receptor Nomenclature, Supplement* **1990**, 25. (b) Lee, C. M.; Iverson, L. L.; Hanley, M. R.; Sandberg, B. E. B. *N. S. Arch. Pharmacol.* **1982**, *318*, 281-287. (c) Laufer, R.; Wormser, U.; Friedman, Z. Y.; Gilon, C.; Chorev, M.; Selinger, Z. *Proc. Natl. Acad. Sci. U.S.A.* **1985**, *82*, 7444-7448. (d) Quirion, R.; Dam, T. V. *Neuropeptides* **1985**, *6*, 191-204. (e) Buck, S. K.; Shatzer, S. A. *Life Sci.* **1988**, *44*, 2701-2705. (f) Regoli, D.; Nantel, F. *Biopolymers* **1991**, *31*, 777-783. (g) Masu, Y.; Nakayama, K.; Takami, H.; Harada, Y.; Kuno, M.; Nakanishi, S. *Nature* **1987**, *329*, 836-838. (h) Yokota, Y.; Yoshiki, S.; Kohichi, T.; Fujiwara, T.; Tsuchida, K.; Shigemoto, R.; Kakizuka, A.; Ohkubo, H.; Nakanishi, S. *J. Biol. Chem.* **1989**, *264*, 17649-17653. (i) Shigemoto, R.; Yokota, Y.; Tsuchida, K.; Nakanishi, S. *J. Biol. Chem.* **1990**, *265*, 623-628.
(4) There are many examples within the peptide field: enkephalins (Schiller, P. W. In *The Peptides*; Udenfriend, S., Meienhofer, J., Eds.; Academic Press: Orlando, FL, 1984; Vol. 6, pp 219-298. Hruby, V. J.; Al-Obeidi, F.; Kazmierski, W. *Biochem. J.* **1990**, *268*, 249-262), somatostatins (Veber, D. H.; Holly, F. W.; Paleveda, W. J.; Nutt, R. F.; Bergstrand, S. J.; Torchiana, M.; Glitzer, M. S.; Saperstein, R.; Hirschmann, R. *Proc. Natl. Acad. Sci. U.S.A.* **1978**, *75*, 2636-2640), thymopoietin (Lautz, J.; Kessler, H.; Boelens, R.; Kaptein, R.; van Gunsteren, W. F. *Int. J. Peptide Protein Res.* **1987**, *30*, 404-414. Kessler, H.; Kutcher, B. *Tetrahedron Lett.* **1985**, *26*, 177-180), and RGD peptides (Aumailley, M.; Gurrath, M.; Müller, G.; Calvete, J.; Timpl, R.; Kessler, H. *FEBS Lett.* **1991**, *291*, 50-54).
(5) (a) Neubert, K.; Hartrodt, B.; Mehlis, B.; Ruger, M.; Bergman, J.; Lindau, J.; Jakubke, H. D.; Barth, A. *Pharmazie* **1985**, *40*, 617. (b) Chassaing, G.; Lavielle, S.; Ploux, O.; Julien, C.; Convert, O.; Marquet, A.; Beaujouan, J. C.; Torrens, Y.; Glowinsky, J. In *Peptides 1984*; Ragnarsson, U., Ed.; Almquist & Wiksell: Stockholm, 1985; p 345. (c) Sandberg, B. E. B.; Bishai, W. R.; Hauna, P. In *Peptides 1984*; Ragnarsson, U., Ed.; Almquist & Wiksell: Stockholm, 1985; p 369. (d) Theodoropoulus, D.; Poulus, C.; Calos, D.; Cordopatis, P.; Escher, E.; Mizrahi, J.; Regoli, D.; Dalietos, D.; Furst, A.; Lee, T. *J. Med. Chem.* **1985**, *28*, 1536. (e) Darman, P.; Landis, G.; Smits, J.; Hirning, L.; Gulya, K.; Yamamura, I.; Burks, T.; Hruby, V. J. *Biochem. Biophys. Res. Commun.* **1985**, *127*(2), 656. (f) Mutulis, F.; Mutulc, I.; Maurops, G.; Seckacis, I.; Grigor'eve, V. D.; Kakaine, E.; Golubeva, V. V.; Myshlyakova, N. V.; Cipens, G. *Bioorg. Khim.* **1985**, *11*, 1276.

0002-7863/92/1514-4818$03.00/0